University of Reading

Projected changes in the Asian-Australian monsoon region in 1.5 °C and 2.0 °C global-warming scenarios

It is advisable to refer to the publisher's version if you intend to cite from the work.

www.reading.ac.uk/centaur

CentAUR

Central Archive at the University of Reading

Reading's research outputs online
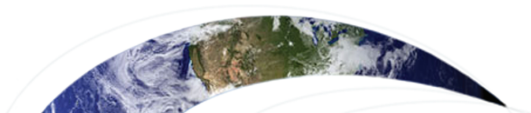
Projected Changes in the Asian-Australian Monsoon Region in 1.5°C and 2.0°C Global-Warming Scenarios

Amulya Chevuturi[1,2] , **Nicholas P. Klingaman[1,2]** , **Andrew G. Turner[1,2]** , **and Shaun Hannah[2]**

[1]NCAS-Climate, University of Reading, Reading, UK, [2]Department of Meteorology, University of Reading, Reading, UK

Abstract In light of the Paris Agreement, it is essential to identify regional impacts of half a degree additional global warming to inform climate adaptation and mitigation strategies. We investigate the effects of 1.5°C and 2.0°C global warming above preindustrial conditions, relative to present day (2006 – 2015), over the Asian-Australian monsoon region (AAMR) using five models from the Half a degree Additional warming, Prognosis and Projected Impacts (HAPPI) project. There is considerable intermodel variability in projected changes to mean climate and extreme events in 2.0°C and 1.5°C scenarios. There is high confidence in projected increases to mean and extreme surface temperatures over AAMR, as well as more-frequent persistent daily temperature extremes over East Asia, Australia, and northern India with an additional 0.5°C warming, which are likely to occur. Mean and extreme monsoon precipitation amplify over AAMR, except over Australia at 1.5°C where there is uncertainty in the sign of the change. Persistent daily extreme precipitation events are likely to become more frequent over parts of East Asia and India with an additional 0.5°C warming. There is lower confidence in projections of precipitation change than in projections of surface temperature change. These results highlight the benefits of limiting the global-mean temperature change to 1.5°C above preindustrial, as the severity of the above effects increases with an extra 0.5°C warming.

1. Introduction

A majority of global and regional surface temperature increases in the 20th and 21st centuries can be attributed to anthropogenic greenhouse gas (GHG) emissions (IPCC, 2014a). Further warming is projected to cause substantial damage to natural and human systems, particularly in less-developed countries. In 2015, the conference of parties (COP) of the United Nations Framework Convention of Climate Change (UNFCCC) concluded with the signing of the Paris Agreement. This agreement focused on strengthening mitigation efforts to limit the global temperature increase above preindustrial conditions to below 2°C, and further to attempt to limit the temperature increase to 1.5°C (UNFCC, 2015). Regional variations in the effects of anthropogenic global warming — and consequently in the benefits of limiting warming to particular thresholds — complicates geopolitical negotiations on targets for emissions and temperature thresholds (Hallegatte et al., 2016; Hulme, 2016; IPCC, 2014b).

Most climate-change research on future projections has examined transient scenarios at periods when global-mean warming substantially exceeds 2°C, to maximize the signal of climate change relative to internal variability, leaving little research focused on the merits of limiting warming to lower thresholds, such as 1.5°C (James et al., 2017; Mitchell et al., 2016). To inform future climate negotiations, UNFCCC requested a special report from the Intergovernmental Panel for Climate Change (IPCC) on the 1.5°C target, which requires focused research on the effects of global warming at 1.5°C versus 2°C or, more generally, on the effects of an additional 0.5°C warming (Rogelj & Knutti, 2016). Scientific research to quantify the regional effects of such climate targets may encourage country-level stakeholders to participate in climate negotiations and to enshrine long-term climate goals in public policy (James et al., 2014; Knutti et al., 2016; Seneviratne et al., 2016).

Most projections of climate-change effects at particular warming thresholds have used model output from emission scenarios (e.g., the representative concentration pathways [RCPs] used for the Coupled Model Intercomparison Project, phase 5 [CMIP5]), by averaging across decadal periods in the simulations with an

average warming at the required threshold (King et al., 2017; Schleussner et al., 2015; Wang et al., 2017). The short averaging period may not be able to link robustly the warming to changes in the mean climate, due to the influence of internal variability, or capture the nonlinear response to global warming through long-term feedbacks (James et al., 2017; Mitchell et al., 2016). Further complications include the presence of a transient warming in the sampling period.

Thus, the Half a degree Additional warming, Prognosis and Projected Impacts (HAPPI) project proposed a modeling approach to project the effects of individual warming thresholds, using atmospheric general circulation models (AGCMs), including uncertainties in projected patterns of temperature change and non-linear responses (Mitchell et al., 2017). The HAPPI approach prescribes sea-surface temperatures (SSTs) and sea ice to constrain simulated global-mean temperature, ensuring constant forcing through the simulation; large ensembles (often more than 100 ensemble members) are performed to quantify robustly the responses of regional climate and weather to the small (0.5°C) difference between the 1.5°C and 2.0°C scenarios (James et al., 2017; Rogelj et al., 2016). Key limitations of this method are that (1) it is difficult to separate model biases and projected changes (James et al., 2017), (2) the 10-year atmosphere-only simulations may not be an accurate representation of the current climate and its variability, and (3) the associated model biases do not always lead to a precise future projection (Lewis et al., 2017).

We focus on the Asian-Australian monsoon region (AAMR) and its three major subregions: East Asia, India, and Australia. This region is characterized by strong, large-scale monsoonal circulations, which directly affect more than 2 billion people, and indirectly affect billions more through its teleconnections to the global circulation. Many studies have analyzed the projected shifts in AAMR mean climate, temperature trends, and spatial and temporal precipitation patterns associated with various emission scenarios (e.g., Hsu, 2016; Hsu et al., 2012; Lee & Wang, 2014; Sillmann et al., 2017; Sperber et al., 2013, 2017, Chapter 7; Wang et al., 2014; Zhang, 2010). All emissions scenarios show very likely increases in surface temperature and frequency of temperature and precipitation extremes over AAMR (Hijioka et al., 2014, Chapter 24; Reisinger et al., 2014). But compared to the East Asian and the Indian monsoon the projected increase of Australian summer monsoon is lower (Wang et al., 2014), with larger uncertainties associated with rainfall variability over Australia as compared to the other two regions (Brown et al., 2017).

Future projections using the emissions-scenario approach (e.g., RCPs from CMIP5) show increased monsoon precipitation over South Asia and East Asia by the late 21st century, including increases in the frequency and intensity of extreme precipitation events, with stronger increases in higher emission pathways (e.g., Brown et al., 2017; Burke & Stott, 2017; Hijioka et al., 2014, Chapter 24; Jourdain et al., 2013; Kitoh et al., 2013; Menon et al., 2013; Reisinger et al., 2014; Sperber et al., 2017, Chapter 7; Turner & Annamalai, 2012; Wang et al., 2014). The enhanced mean monsoon over the tropics is connected to increased moisture availability due to stronger evaporation from the Indian Ocean, Arabian Sea and Bay of Bengal (Lee & Wang, 2014; May, 2011), which also enhances extreme precipitation (Allan & Soden, 2008). Future projections suggest increases in the land-sea and Northern-Southern Hemisphere temperature contrasts: the former leads to increased precipitation over whole of AAMR due to the resulting increased sea-level pressure gradients (Wang et al., 2014); the latter causes a northward shift in AAMR monsoon circulation, leading to enhanced rainfall over South and East Asia and reduced rainfall over Australia (Cherchi et al., 2011; Hu et al., 2000; Menon et al., 2013). The equatorial Pacific mean SST response to warming may resemble El Niño, with greater warming in the eastern Pacific than in the western (e.g., Tokinaga et al., 2012), leading to anomalous subsidence over Australia and reduced precipitation.

However, only a few studies have analyzed the effects on the AAMR of particular global-mean temperature targets of limiting the global warming to 1.5°C over preindustrial levels. Schleussner et al. (2015) estimated the impacts of 1.5°C versus 2°C warming using CMIP5 outputs. They projected increased intensity and duration of heat extremes throughout the tropics, and increased intensity in precipitation extremes over South Asia in the 2°C scenario, among many other impacts. King et al. (2017) showed statistically significant increases in the likelihood of heat extremes over Australia in a 2.0°C scenario, relative to 1.5°C, using CMIP5 data, but found less-coherent changes in the frequency of precipitation extremes. These studies suggest substantial effects of a further 0.5°C of global-mean warming (Schleussner et al., 2015). Lewis et al. (2017) used HAPPI projections to show that heat extremes in Australia may increase by twice the global-mean warming; CMIP5 projections also show an increase in the occurrence of heat extremes.

This study contributes to the evaluation of the effects of 1.5°C and 2.0°C global-warming above preindustrial conditions, focusing on the AAMR, based on HAPPI model experiments. We assess projected changes over the AAMR and its subregions in the two future scenarios by (1) evaluating the shifts in the mean climate (for temperature, precipitation, and circulation) and (2) identifying changes in the intensity, frequency, and persistence of temperature and precipitation extremes. In Section 2, we describe the datasets used (Section 2.1), the study region (Section 2.2) and our analysis method (Section 2.3). Section 3 describes the results of model validation (Section 3.1), projected changes in mean climate (Section 3.2) and extreme events (Section 3.3). We conclude our study in Section 4.

2. Methods

2.1. Data

We analyze AGCM simulations from the HAPPI Tier-1 experiments (Mitchell et al., 2017). The experiment design comprises three scenarios with variations to prescribed SSTs, sea ice and GHG and aerosol forcing. Each experiment has a different imposed global-mean warming relative to the reference preindustrial period (1861–1880). The three experiments are:

All-Hist: The most recent decade, spanning 2006–2015. This experiment is ≈0.8°C warmer than the preindustrial. Observed SST from 2006 to 2015 are prescribed for the All-Hist simulations.
Plus-1.5: The 1.5°C scenario, which is 1.5°C warmer than the preindustrial and 0.7°C warmer than All-Hist. The boundary conditions for this experiment are provided from RCP2.6 of CMIP5. Projected SSTs for Plus-1.5 are the sum of the observed SSTs used for All-Hist and the mean difference between the CMIP5 decadal averages of SSTs between the recent decade (2006–2015) and a world 1.5°C warmer than the preindustrial.
Plus-2.0: The 2.0°C scenario, which is 2.0°C warmer than the preindustrial and 1.2°C warmer than All-Hist. The boundary conditions for this experiment are a weighted average of RCP2.6 and RCP4.5 of CMIP5. Projected SSTs for Plus-2.0 are the sum of the observed SSTs used for All-Hist and the difference between the CMIP5 decadal averages of SSTs between the recent decade and a 2.0°C warmer world (relative to preindustrial).

We analyze data from large ensemble simulations of five AGCMs for which quality-controlled data were available; details are provided in Table 1. The number of ensemble members varies between AGCMs, but all have ≥100 members; the members differ only in their initial conditions. The large ensemble approach is designed to capture the potentially small changes in regional climate between the scenarios, relative to internal atmospheric variability, and to quantify robustly the potential changes in extreme events with large samples. These experiments have relatively short 10-year simulations, which are designed to reduce computational expense while still permitting analysis of interannual variability and extremes, but which cannot represent decadal variability (James et al., 2017; Mitchell et al., 2017).

To evaluate systematic model errors in the HAPPI AGCMs, we validate the All-Hist simulated mean climate and extreme intensity against observations, for 2006–2015 to coincide with period of the All-Hist forcing. We evaluate monthly near-surface temperature against the Hadley Centre/Climatic Research Unit temperature dataset (HadCRUT4), version 4.6.0.0, which is the combined land (CRUTEM4) and marine SST (HadSST3) on a 5° × 5°-grid (Morice et al., 2012). We evaluate the extreme daily maximum near-surface temperature against the European Centre for Medium Range Weather Forecasts Interim reanalysis (ERA-Interim) daily maximum 2 m temperature at 0.75° × 0.75° resolution (Dee et al., 2011). We evaluate daily and monthly precipitation against the Global Precipitation Climatology Project (GPCP), version 2.3, precipitation dataset with combined observations and satellite precipitation data at 2.5° × 2.5° grid (Adler et al., 2003). We evaluate 850 hPa winds against ERA-Interim.

2.2. Study Area

The region of interest covers the AAMR (30°E–180° and 60°S–60°N). We divide the AAMR into three regions: (1) the East Asian monsoon region (95°–165°E and 0°-55°N; hereafter EA), (2) the Indian monsoon region (55°–95°E and 0°–35°N; hereafter IND) and (3) the Australian monsoon region (95°–165°E and 45°S–0°; hereafter AUS), as depicted in Figure 1f. We further divide each region into two subregions based on areas of high monsoonal precipitation over land (Figure 1f): EA1 (north-eastern China) and EA2 (southern China and south-east Asia); IND1 (southern India) and IND2 (northern India, Pakistan and Nepal); AUS1

Table 1.

Details of the Models from the HAPPI Project Analyzed in This Study

Model	Name	Institute	Grid Resolution (grid-points)	Ensemble Members	Reference
Community atmosphere model 4-2°	CAM	ETH[a]	2° × 2° (96 × 144)	501	Neale et al. (2013)
Canadian Fourth generation atmospheric global climate model	CAN	CCCma[b]	T42 (64 × 128)	100	von Salzen et al. (2013)
ECHAM6.3-LR	ECH	MPI-M[c]	T63 (96 × 192)	100	Stevens et al. (2013); Reick et al. (2013)
Model for interdisciplinary research on climate 5	MIR	AORI[d], NIES[e], JAMSTEC[f]	150 × 150 km (128 × 256)	100	Watanabe et al. (2010); Shiogama et al. (2014)
Norwegian earth system model 1	NOR	NCC[g]	1.25 × 0.94° (192 × 288)	125	Bentsen et al. (2013); Iversen et al. (2013); Kirkevåg et al. (2013)

Note. We analyzed only those models for which quality-controlled data were available at the time of this study. For each model, we list the name of the model, the abbreviation used in the text, the institute that performed the simulation, the horizontal grid resolution in degrees (with corresponding number of latitude × longitude gridpoints in parentheses), the number of ensemble members and a reference for further details.
[a]Federal Institute of Technology; Zurich, Switzerland.
[b]Canadian Centre for Climate Modeling and Analysis; Victoria, Canada.
[c]Max Planck Institute for Meteorology; Hamburg, Germany.
[d]Atmosphere and Ocean Research Institute, University of Tokyo; Chiba, Japan.
[e]National Institute for Environmental Studies; Ibaraki, Japan.
[f]Japan Agency for Marine-Earth Science and Technology; Kanagawa, Japan.
[g]NorESM Climate modeling Consortium, Norway.

(north-western Australia) and AUS2 (north-eastern Australia). We choose our regions and subregions after reviewing research that identified each region's distinct climatological monsoon precipitation patterns (e.g., Christensen et al., 2013; Wang et al., 2012; WCRP, 2017; Zhang, 2010).

2.3. Methodology

To understand the changes in Plus-1.5 and Plus-2.0, we analyze the monthly near-surface air temperature (TAS) and daily and monthly precipitation (PR), daily maximum surface air temperature (TASMAX), and monthly 850 hPa winds. We use monthly data to assess annual-mean and seasonal-mean changes; we use daily data to assess changes in extreme events. For seasonal-mean changes, we focus on the wet (monsoon) season in each region (JJA for IND and EA, DJF for AUS). We also analyze changes in the intensity and persistence of extreme events using several indices, which will be described in detail alongside the analysis. We analyze changes using the individual ensemble members from each AGCM, not only the ensemble mean. We use paired Student's *t*-tests to evaluate the statistical significance of changes. Area averages are computed over each region and subregion (Figure 1f), using the land points only. We also use IPCC terminology to define uncertainty of our results in terms of confidence (based on intermodel agreement) and likelihood (based on intraensemble agreement). Due to the high number of ensemble members per model, the likelihood of future change can be assessed with greater accuracy; with only five models, however, it is difficult to robustly quantify the intermodel uncertainty in projected changes.

3. Results

3.1. Model Validation

Before examining the projected changes in Plus-1.5 and Plus-2.0, we briefly validate the AAMR mean climate and extremes in All-Hist against observations, as described in Section 2.1, as model biases may influence
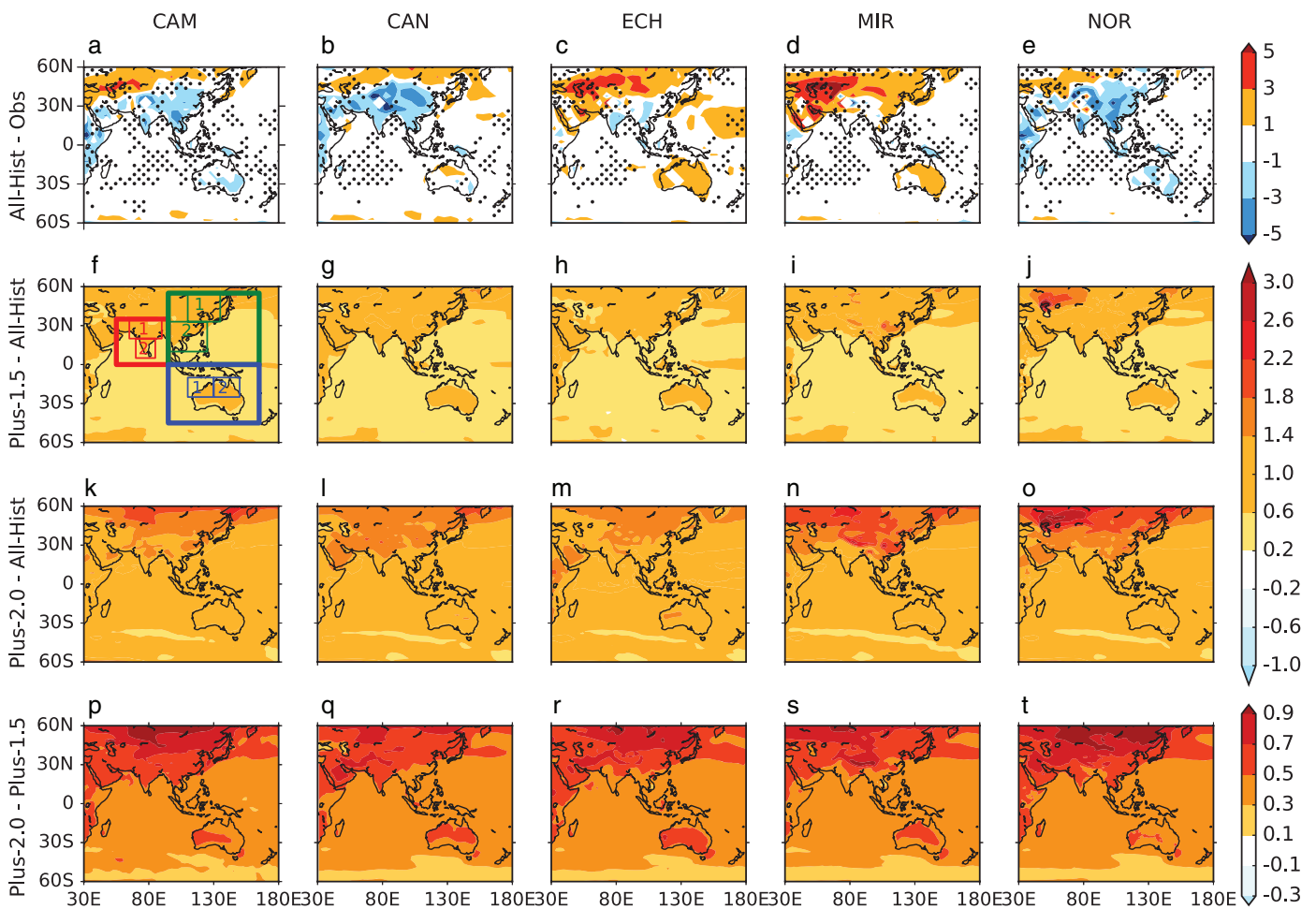
Figure 1. Annual-mean TAS differences (K) in the ensemble-mean of each model between (a–e) All-Hist and HadCRUT4, (f–j) Plus-1.5 and All-Hist, (k–o) Plus-2.0 and All-Hist, (p–t) Plus-2.0 and Plus-1.5. The stippling shows regions which are *not* statistically significant at the 95% confidence level. In panel (f), the regions and subregions used in the study are marked as: the East Asian monsoon region (EA) and subregions (EA1 and EA2) in green, Indian monsoon region (IND) and subregions (IND1 and IND2) in red and the Australian monsoon region (AUS) and subregions (AUS1 and AUS2) in blue.

future projections (e.g., Reichler & Kim, 2008). For annual-mean TAS, all models show near-zero biases over the oceans due to the prescribed SSTs (Figures 1a–1e); biases are not exactly zero due to our use of a different validation dataset to that used for the HAPPI SST forcing, as well as intermodel variations in the difference between SST and TAS. For Northern Hemisphere (NH) land, most models are biased cold in the tropics and biased warm in the subtropics and extra-tropics. For Southern Hemisphere (SH) land, there is intermodel variability in biases across Australia, with CAM and NOR showing a cold bias, whereas the other three models have warm biases.

Model biases in monsoon-season precipitation vary across the AAMR (Figures 2a–2e). All models have a significant wet bias in EA compared to observations; the bias varies in spatial extent. AUS shows a significant wet bias in CAM, MIR, and NOR and a slight dry bias or no significant bias in CAN and ECH. Strong significant precipitation biases are found across the IND region, with intermodel and interregion variation, resulting in wet biases in some models and subregions and dry biases in others. These errors in precipitation may be stronger in AGCMs than coupled models due to a lack of coupled ocean-atmosphere feedbacks, which have been demonstrated to be important for monsoon precipitation (e.g., Jourdain et al., 2013; Sperber et al., 2013; Wang et al., 2005).

Models reproduce well the general monsoon circulation over the AAMR, though with some substantial biases (Figures 3a–3e). EA (except EA1) shows a southerly bias; IND and EA1 has a strong westerly bias.
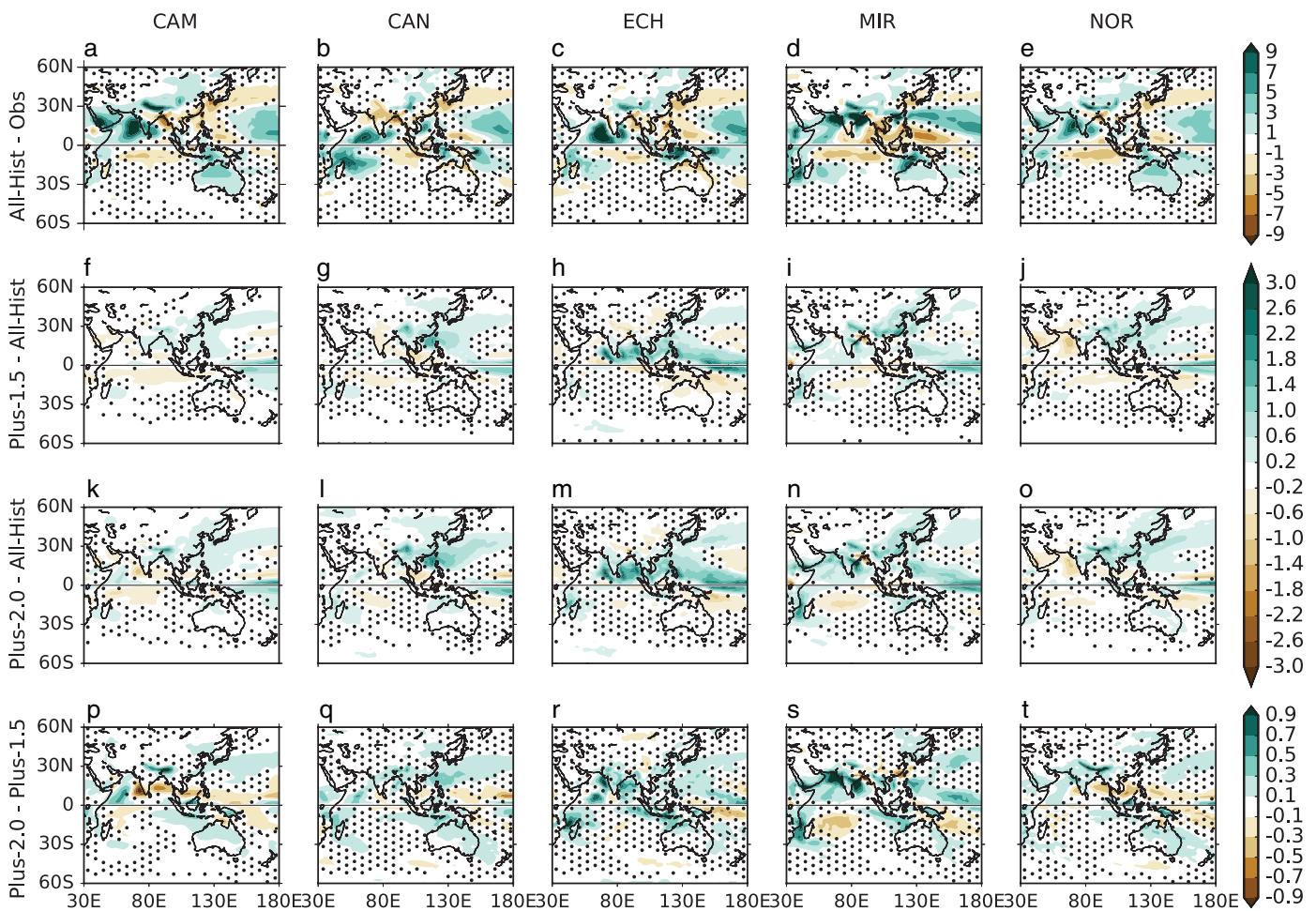
Figure 2. As in Figure 1, but for precipitation change (mm day^{-1}) for the monsoon season: JJA in the NH and DJF in the SH. Note that this introduces a break in the data at the equator, where the season changes. Observations in (a–e) are GPCP.

These circulation biases result in excessive monsoon flow over these regions and are associated with positive precipitation biases. There is a clear anomalous cyclonic circulation over western AUS, which varies in strength among models. There are intermodel differences in circulation biases over India and southeast Asia, with enhanced flow in MIR and reduced monsoon circulation in CAN, associated with a wet and dry bias, respectively (Figures 2b and 2d). These circulation biases are common in AGCMs and may arise in part from a lack of air-sea interactions (e.g., He et al., 2016; Wang et al., 2004; Zhou et al., 2008).

We analyze the area-average bias (land only) for each region and model, as well as the percentage of ensemble members that agree with the sign of the ensemble-mean bias and the statistical significance of the bias, for TAS (Figure 4a) and precipitation (Figure 4e). MIR and ECH showing a consistent warm bias over all regions; IND2 region has a cold bias in all models. All regions and all models show a wet bias, except for IND and AUS in CAN and ECH.

All models show a warm bias for extreme daily maximum near surface temperature (99th percentile; Figures 7a–7e) over IND when compared with ERA-Interim. For EA and AUS three models show a warm bias: CAM and NOR show a cold bias over AUS whereas CAM and ECH show a cold bias over parts of EA. The extreme temperature bias is significant over most land points except over EA in NOR. There is intermodel variability in the extreme daily precipitation (99th percentile) bias over the AAMR against GPCP data (Figures 8a–8e). There is a significant wet bias over EA1 in all five models, whereas EA2 and IND1 show a dry bias in all models except MIR, which is not always significant. AUS shows a dry bias in extreme precipitation in CAN and ECH, a wet bias in MIR and NOR and mixed signals in CAM. These substantial biases in mean and
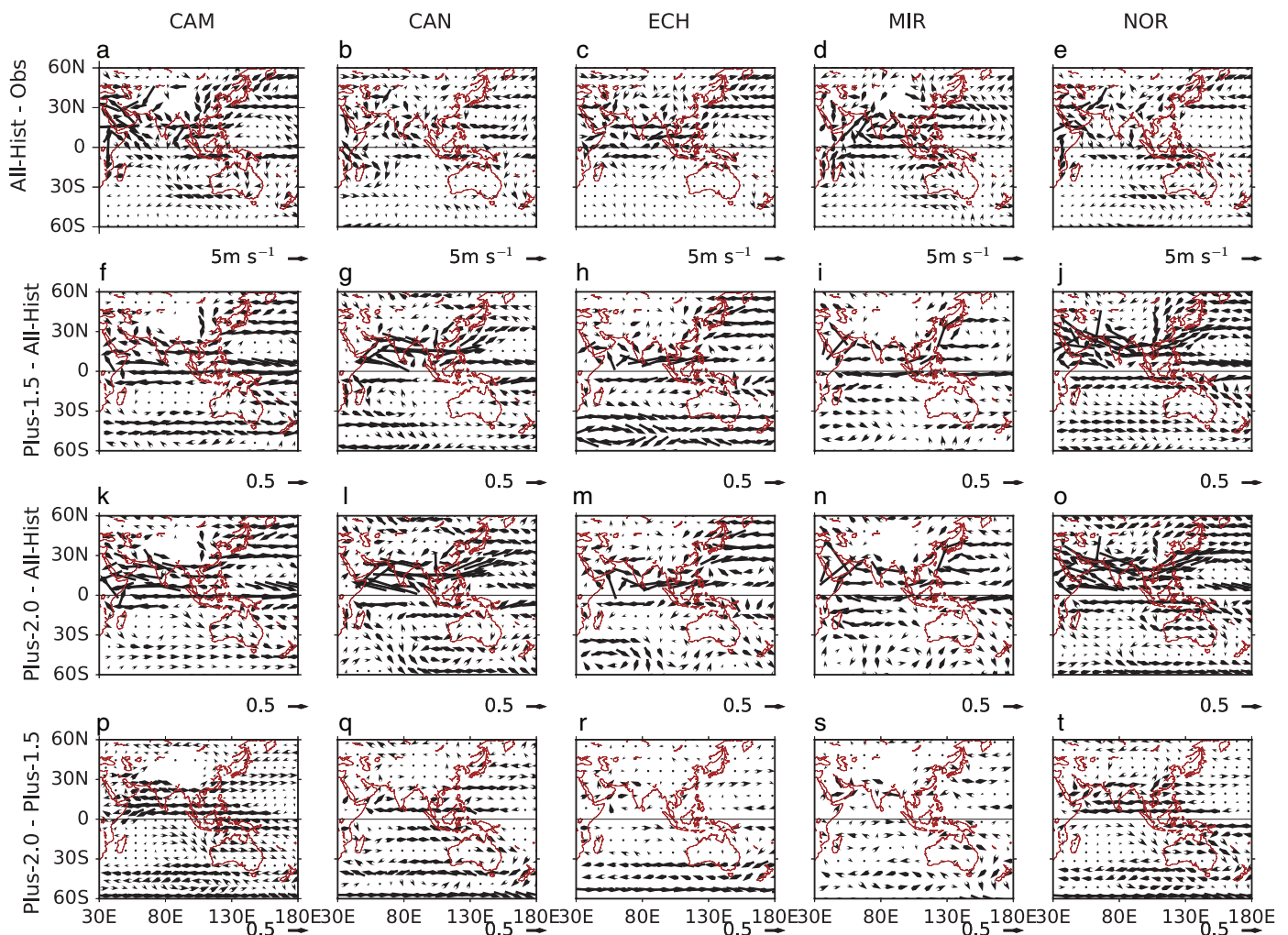
Figure 3. As in Figure 5, but for 850 hPa winds (m s^{-1}). Observations in (a – e) are ERA-Interim.

extreme temperature and precipitation in All-Hist suggest that future projections should be interpreted with a degree of caution, particularly given the limited number of models in the HAPPI dataset.

3.2. Projected Changes in Mean Climate

Overall, the AMMR climate is projected to significantly warm in both Plus-1.5 (Figures 1f – 1j) and Plus-2.0 (Figures 1k – 1o). Warmer climates are projected by all studies of increased emissions scenarios (IPCC, 2014a). Warming is greater at higher altitudes, the Tibetan Plateau, Himalayas and Western Australia (Figures 1p – 1t), possibly due to complex interactions of factors such as albedo, cloud and radiative feedbacks (Pepin et al., 2015). Intermodel variations over the ocean are very small, due to the prescribed SST. Over the AAMR, the NH (EA and IND) warms more than the SH (AUS), due to asymmetry of land area between hemispheres (Lee & Wang, 2014). Furthermore, TAS over land is significantly warmer in the future scenarios compared to All-Hist, with approximately 1.8°C warming over land in Plus-2.0 (cf. a global-mean warming of 1.2°C) and approximately 1.0°C warming in Plus-1.5 (c.f. a global-mean warming of 0.7°C), as shown in Figures 4a – 4e.

To understand the uncertainties associated with the model simulations, we analyze the area average TAS over land for all ensemble members for each scenario (Figures 4b – 4d and 5a – 5e). There is very high confidence and virtual certainty for increased temperatures in EA, IND (>0.7°C for ensemble mean) and AUS (>0.5°C) in Plus-1.5, since all ensemble members exceed the All-Hist ensemble-mean for all models. There is also very high confidence and virtual certainty in projected increased temperatures over EA (≈1.5°C), IND
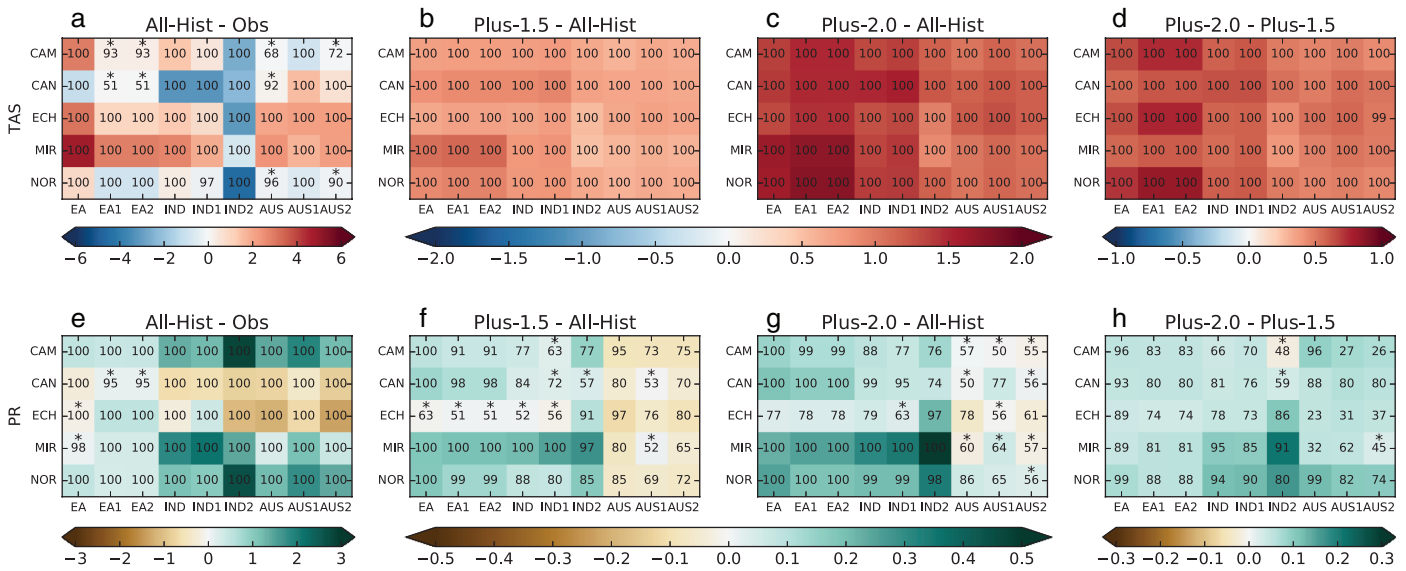
Figure 4. Panels (a–d) show annual TAS differences (K) for (a) All-Hist minus HadCRUT4, (b) Plus-2.0 minus All-Hist (c) Plus-1.5 minus All-Hist, (d) and Plus-2.0 minus Plus-1.5 for all regions (EA, IND, AUS) and subregions (EA1, EA2, IND1, IND2, AUS1, AUS2) and all five models for land only. Shading shows the change in the ensemble mean. The numbers in each box represent the percentage of ensemble members in which the sign of the change agrees with the sign of ensemble-mean change. The * symbol represents ensemble-mean differences that are *not* significant at the 95% confidence level. Panels (e-h) are as for (a–d) but for annual-mean precipitation differences (mm day^{-1}), using GPCP as observations.

(≈1.0°C), and AUS (≈0.7°C) for Plus-2.0 versus All-Hist, as well as over AAMR land (≥0.5°C) for the difference between Plus-2.0 and Plus-1.5.

Previous modeling studies show that globally, monsoon precipitation increases with warming, particularly over the AAMR (e.g., Christensen et al., 2013; Hsu et al., 2012; Lee & Wang, 2014; Wang et al., 2014). Using ensemble-mean changes, monsoon-season precipitation is projected to increase in Plus-1.5 (Figures 2f–2j) and Plus-2.0 (Figures 2k–2o) over EA and IND in most models, but there is little to no change over AUS. In Plus-1.5, ECH is the only model to simulate drying over some parts of all three regions, while CAN is the only model to show wide-spread, significant drying over IND. Comparisons of Plus-2.0 against Plus-1.5 show significantly wetter conditions in all models and subregions. Precipitation increases over AUS are weaker as compared to IND and EA for Plus-2.0, consistent with the smaller changes in precipitation over AUS in Plus-1.5.

In RCP8.5 emission scenarios, models project a significant increase in monsoon precipitation in all regions by 2100 (IPCC, 2014b), but in RCP4.5 the projected increases are stronger in EA and IND than in AUS, which shows greater uncertainty in the sign of change (e.g., Christensen et al., 2013; Hulme et al., 1994; Irving et al., 2012; Jourdain et al., 2013; Menon et al., 2013; Wang et al., 2014), which is consistent with our analysis (Figure 2). From our analysis of the ensemble range of seasonal precipitation changes (Figures 5f–5j), we note that there is high confidence in the increase of monsoon precipitation over EA (≈0.3 mm day^{-1}) in Plus-1.5, which is virtually certain. There is medium confidence in the increase of monsoon precipitation over IND (≈0.1 mm day^{-1}) in Plus-1.5, which is projected to be likely; there is no clear change over AUS. The ensemble ranges of Plus-1.5 and Plus-2.0 overlap with the All-Hist ensemble range, suggesting that the changes in precipitation do not exceed the range of present-day internal variability. Such uncertainty in model precipitation responses to the relatively small temperature increases was also noted by King et al. (2017) for AUS. In the annual mean, AUS is projected to likely dry (≈0.1 mm day^{-1}) in Plus-1.5 (very high confidence, Figure 4g), but there is low confidence in the sign of change for Plus-2.0 (Figure 4h). Overall, there is high confidence in the increase of annual precipitation between Plus-1.5 and Plus-2.0 for AAMR; increases are likely (≈0.1 mm day^{-1}) over EA and IND, but increases and decreases are approximately equally likely for AUS.

Previous climate-change projections suggest an enhanced Hadley circulation and a weaker Walker circulation with warming (e.g., Lee & Wang, 2014; Tokinaga et al., 2012; Turner & Annamalai, 2012), however the responses of regional monsoon circulations are often more complex and uncertain (e.g., Schneider et al.,
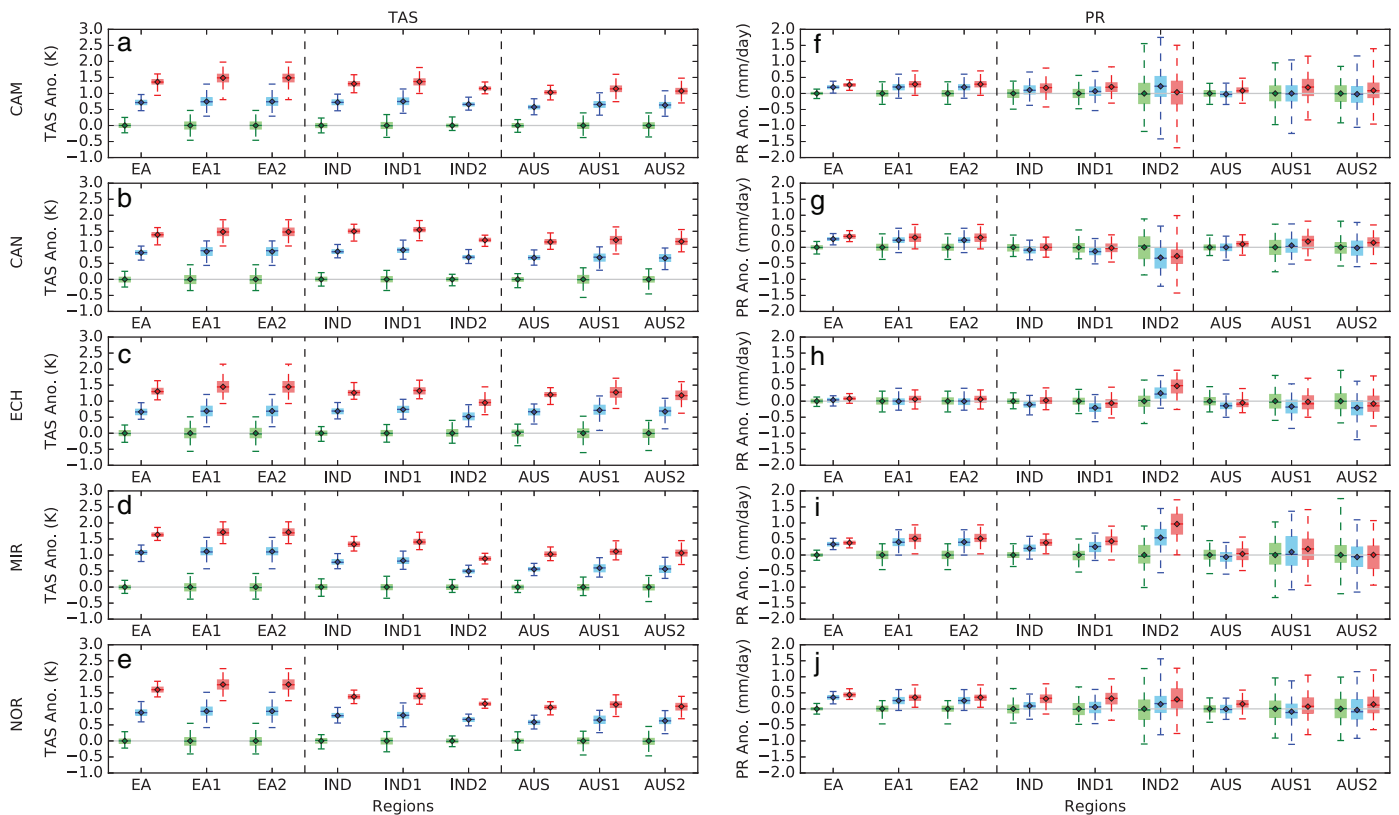
Figure 5. Annual TAS anomaly (K) in the left column and monsoon season precipitation (PR) anomaly (mm day⁻¹) in the right column for each scenario All-Hist (green), Plus-1.5 (blue) and Plus-2.0 (red) for all regions (EA, IND, AUS) and subregions (EA1, EA2, IND1, IND2, AUS1, AUS2). For each variable (TAS and PR), the anomaly is computed from its respective All-Hist ensemble mean. The diamonds show the ensemble mean anomaly and the boxplots show the spread of anomalies from the ensemble members of each scenario. For each boxplot; whiskers show the range (max−min) of the anomalies, middle dash is the median and box-ends show interquartile range of the ensemble members. Different models are shown in (a,f) CAM, (b,g) CAN, (c,h) ECH, (d,i) MIR and (e,j) NOR.

2010; Vecchi et al., 2006; Wang et al., 2004). In Plus-1.5, over AUS the monsoon flow either weakens or shows little change compared to All-Hist (Figures 3f–3j). The weaker north-westerly flow is associated with drying over AUS, especially over northern Australia; this feature is most pronounced in ECH. Conversely, in all models Plus-2.0 shows a slightly stronger Australian monsoon circulation than Plus-1.5 (Figures 3p–3t). In the RCP 4.5 scenario in CMIP5 simulations, there is also weak enhancement of north-westerly flow over AUS (Wang et al., 2014), but these projected changes in circulation are uncertain (Lee & Wang, 2014). Over EA, in EA2 the monsoon circulation strengthens through enhanced southerly and westerly flow in Plus-1.5 (Figures 3f–3j) and Plus-2.0 (Figures 3h–3l) compared to All-Hist, associated with increased precipitation. EA1 shows an easterly anomaly. As a whole, EA shows enhanced precipitation in the future scenarios, due to the enhanced south-easterlies over the South China Sea and easterlies over western north Pacific, which are associated with a stronger western north Pacific monsoon trough and enhanced convergence. These changes over EA1 and EA2 are more pronounced in Plus-2.0 than in Plus-1.5 (Figures 3p–3t). The enhancement of the southeasterlies over EA (Wang et al., 2014) and westward migration of the western north Pacific circulation (Lee & Wang, 2014) is also projected by the RCP 4.5 scenario in CMIP5 simulations.

The circulation response over IND varies considerably among the HAPPI models, related to the variability in precipitation changes. In Plus-1.5, CAM and NOR show an anomalous cyclonic circulation over Indian land (Figures 3f and 3j), strengthening the climatological monsoon flow; these models also show increased precipitation over IND2, but reduced precipitation off the west coast of India (Figures 2f and 2j). Similar but amplified patterns of circulation (Figures 3k and 3o) and precipitation (Figures 2k and 2o) changes are seen in Plus-2.0. CAN displays enhanced anomalous easterly flow over the Arabian Sea in the future scenarios (Figures 3g and 3l), weakening the climatological westerly flow. These circulation changes are associated

with reduced precipitation in Plus-1.5 (Figure 2g). Plus-2.0 shows a smaller drying signal (Figure 2l), possibly due to increased tropospheric water vapor counteracting the circulation changes. In ECH (Figure 3h) and MIR (Figure 3j) the monsoon circulation shifts southwards and northwards, respectively in Plus-1.5. Such shifts are linked to shifts in monsoon precipitation, particularly over the Himalayas, where precipitation is significantly reduced in ECH (Figure 2h) and enhanced in MIR (Figure 2j). The southward shift of the monsoon circulation in ECH also leads to anomalous convergence over IND2, enhancing precipitation significantly. In Plus-2.0 the monsoon circulation over IND shifts slightly northwards in ECH (Figure 3r) and MIR (Figure 3t), relative to Plus-1.5. CMIP5 models show a similar northward shift in the low level monsoon circulation and vorticity with the high emission RCP-8.5 scenario (Menon et al., 2013). This poleward shift is perhaps caused due to a broadening of the tropics and poleward shift of mid-latitude jet streams and associated changes in the spatial extent of precipitation (Sandeep & Ajayamohan, 2015).

Whether regional effects of climate change scale linearly with the global-mean temperature increase is a key question in climate-change science, as a linear relationship would allow extrapolation of simulated or observed changes to a range of potential warming levels. To assess whether mean precipitation changes scale with the global-mean surface temperature change, we calculate the ratio of the mean precipitation change for each warming scenario, relative to All-Hist, for each grid-point, to the global-mean surface temperature change in that experiment ($\Delta p/\Delta \overline{T}$, hereafter PT). We then compare PT for Plus-2.0 against PT for Plus-1.5 (Figure 6). Precipitation change scales sublinearly with global-mean temperature change for all models, globally and for the AAMR. This demonstrates a stronger change in precipitation per unit warming in Plus-1.5 than in Plus-2.0. Only IND in CAM shows little to no precipitation change with warming. Our results are consistent with previous studies that have found that low-level moisture availability scales more linearly with warming in models (as per the Clausius-Clapeyron relation) than the regional hydrological response, which depends on radiative and evaporative constraints as well as moisture content (e.g., Allen & Ingram, 2002; Vecchi et al., 2006). Thus, models often show sublinear scaling of precipitation in response to the surface temperature increase, especially in the tropics, due changes in regional moisture transports (e.g., Held & Soden, 2006; Schneider et al., 2010; Sillmann et al., 2017).

3.3. Projected Changes in Extreme Events

IPCC reports indicate a high likelihood of increasing temperature and precipitation extremes over the AAMR (e.g., Christensen et al., 2013; Collins et al., 2013). The regional responses of the mean climate and extremes to global warming often differ (Seneviratne et al., 2012), due to different dynamic and thermodynamic forcings (Emori & Brown, 2005). Thus, in this subsection, we analyze changes in the intensity and persistence of extreme events in the future scenarios.

Changes in the intensity of extreme (99th percentile) daily TASMAX in Plus-1.5 and Plus-2.0 are shown in Figure 7. As expected, projected changes in the intensity of temperature extremes are significantly higher (very high confidence) in Plus-2.0 compared to Plus-1.5 across the whole AAMR by at least 0.7°C (Figures 7k–7o). There is high confidence in the increased intensity of heat extremes in Plus-2.0, particularly over the higher latitudes of the EA and in the climatologically coldest regions (parts of Tibetan Plateau and Gobi Desert), where the increase is >1°C against Plus-1.5. The increase in intensity of TASMAX is 0.5°C over most AUS but only 0.2°C increase over SE Australia with additional 0.5°C global warming (Figures 7k–7o), which is projected with high confidence. The greater-than-double increase in the magnitude of the extreme temperatures over Australia with the 2.0°C warmer HAPPI scenario was also shown by Lewis et al. (2017).

To understand the changes to the temperature extremes, we analyze frequency histograms of daily TASMAX (bars in Figure S1, Supporting Information), and the percentage change of frequency in Plus-1.5 and Plus-2.0 with respect to All-Hist (lines in Figure S1). For EA (Figures S1a–S1e), the histograms are strongly negatively skewed, due to the relatively colder regimes in winter, compared to IND (Figures S1f–S1j) and AUS (Figures S1k–S1o). For each region, below 300 K the percentage differences in Plus-1.5 and Plus-2.0 are negative, showing reduced frequencies of colder TASMAX in future scenarios (very high confidence). Such reductions, particularly in Plus-2.0, have been shown in previous studies of 2°C warmer worlds (Seneviratne et al., 2012), but further analysis with daily minimum temperature is required to understand the changes in the cold temperature extremes. Beyond 300 K TASMAX, the change in Plus-1.5 and Plus-2.0 becomes positive; the increase in Plus-2.0 is higher, especially in the higher TASMAX range. Thus, there is high confidence
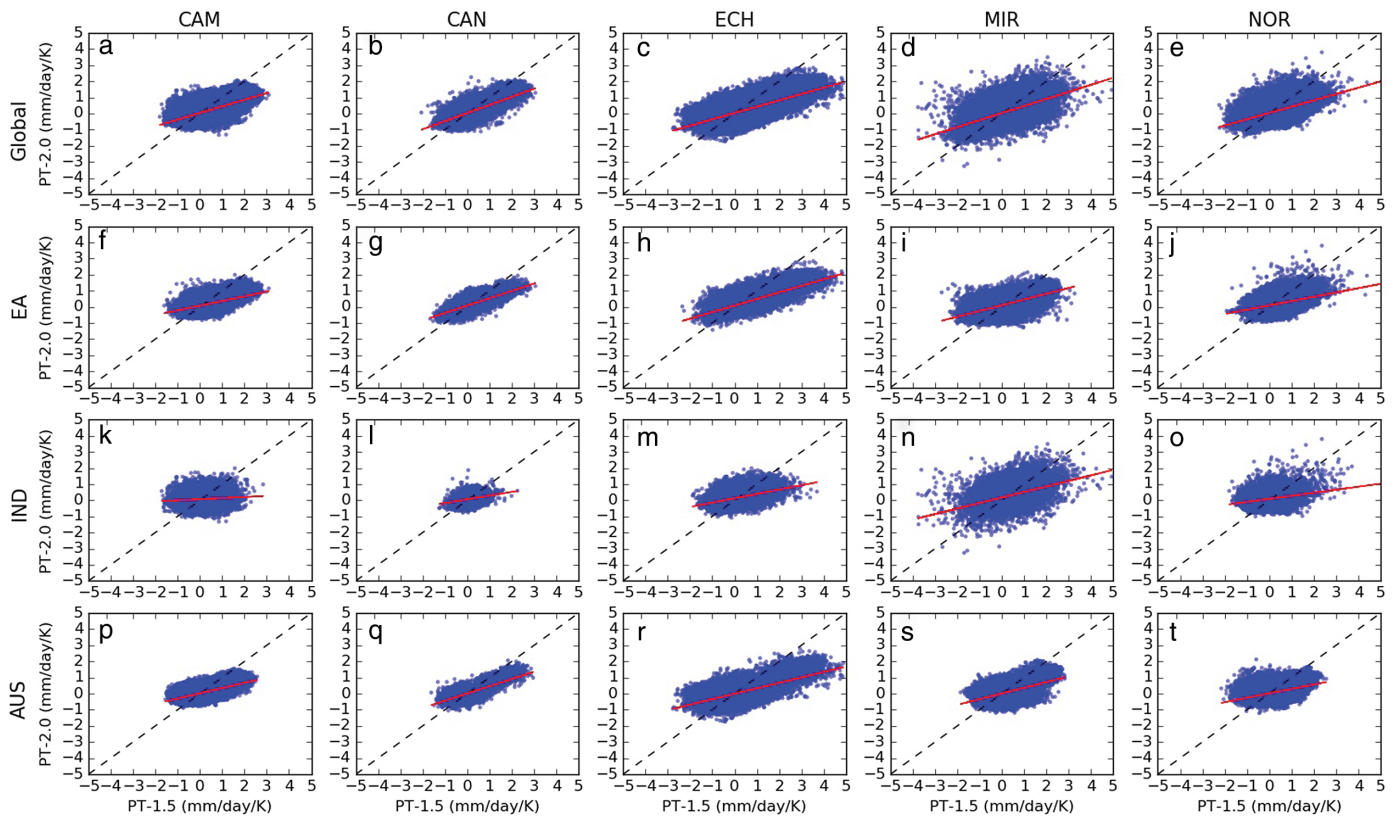
Figure 6. Ratio of monthly change in precipitation climatology and global surface temperature change; PT ($\Delta p / \Delta \overline{T}$; mm day^{-1} K^{-1}) at each grid-point for Plus-2.0 (PT-2.0; y-axis) versus Plus-1.5 (PT-1.5; x-axis) scenarios as blue points with the linear fit regression line of the scatter plot shown in red. Each column represents a model: CAM (a,f,k,p), CAN (b,g,l,q), ECH (c,h,m,r), MIR (d,i,n,s), NOR (e,j,o,t). Each row represents a region: Global (a–e), EA (f–j), IND (k–o), and AUS (p–t).

in projected increase of at least 20% in the strongest heat extreme frequency over AAMR due to an additional 0.5°C warming. On analyzing the percentage of ensemble members that agree with the sign of the ensemble-mean change (Figure S3), we note that changes in the frequency of TASMAX are likely for almost all temperature ranges over EA (Figures S3a–S3e) and AUS (Figures S3k–S3o), with changes in frequency over 300 K are virtually certain for EA with additional 0.5°C warming and very likely for EA with very high confidence. For IND (Figure S3), the likelihood of change varies at different temperature ranges; and change for greater than 300 K are likely for any additional warming, with high confidence. Schleussner et al. (2015) also report significant increases in heat-related extremes over the tropics for an additional 0.5°C warming, with Lewis et al. (2017) showing likely increases of temperature extremes over Australia under the RCP 8.5 scenario by mid-late 21st century.

There is higher uncertainty in the projections of precipitation extremes (Figure 8) than for temperature extremes. Increased intensity of precipitation extremes over monsoon regions is expected in a warmer world (e.g., Alexander & Arblaster, 2009; Burke & Stott, 2017; Hijioka et al., 2014, Chapter 24; Reisinger et al., 2014; Seneviratne et al., 2012; Turner & Slingo, 2009). In Plus-2.0, EA and IND show significant increases in the intensity of precipitation extremes (high confidence), but there is only medium confidence in the projected increase for AUS (Figures 8f–8j). ECH projects reducing intensity of extreme precipitation over parts of AAMR in Plus-1.5 (Figure 8c). The additional 0.5°C warming leads to significant increases in extreme precipitation projections (high confidence) only in EA1 and IND1 (Figures 8k–8o). There is only medium confidence in the projections for EA2, IND2, and the AUS subregions. Schleussner et al. (2015) suggest 0.5°C warming leads to increasing extreme precipitation intensity over EA, but not IND and AUS. King et al. (2017) reported high uncertainty in projections of precipitation extremes over AUS in the 1.5°C scenario.
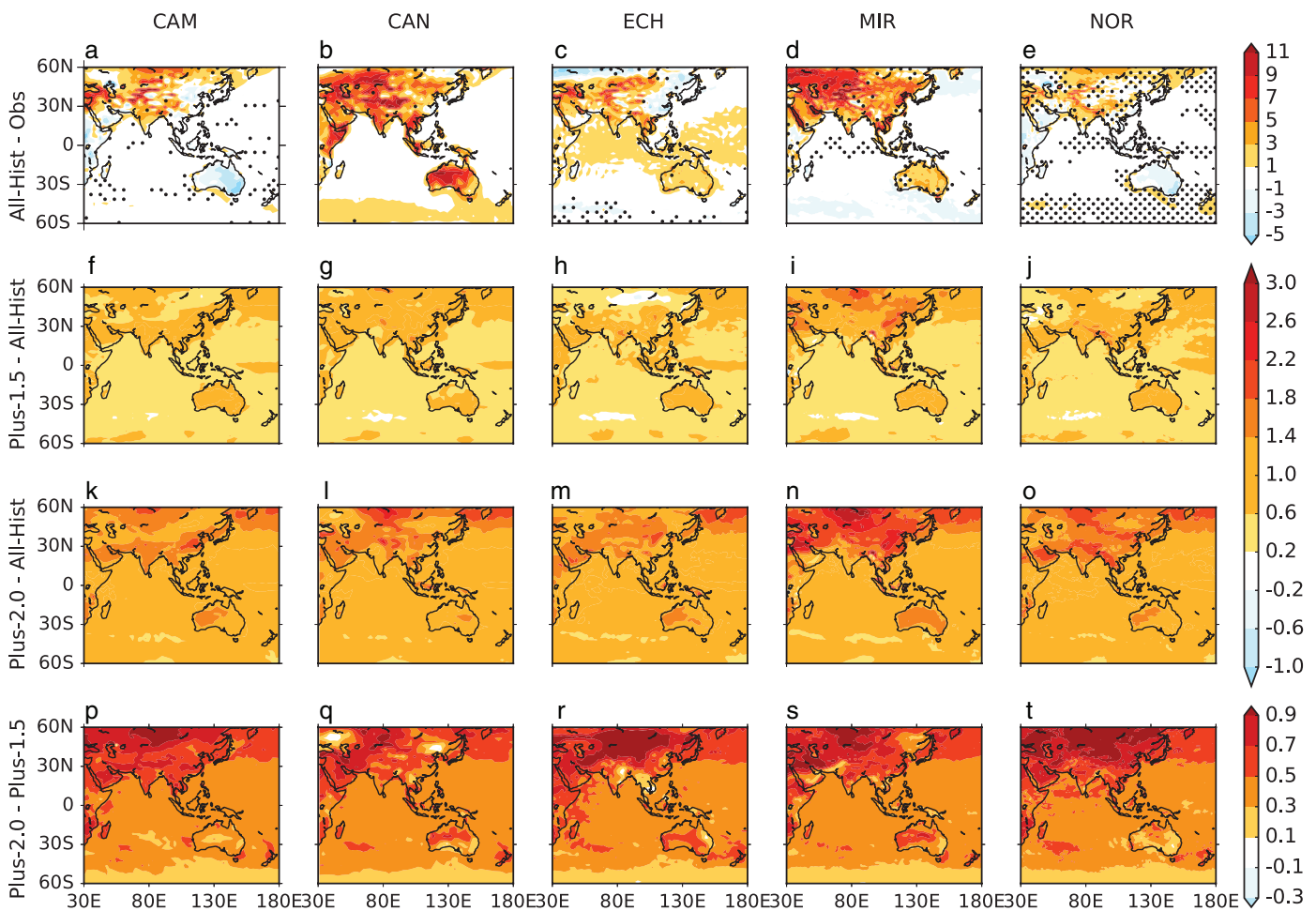
Figure 7. Change in the 99th percentile of daily maximum surface temperatures (K) in the ensemble-mean of each model between (a–e) All-Hist and ERA-Interim, (f–j) Plus-1.5 and All-Hist, (k–o) Plus-2.0 and All-Hist, and (p–t) Plus-2.0 and Plus-1.5 for all five models. Stippling shows regions which are *not* statistically significant at the 95% confidence level.

Changes in the frequency histograms for daily PR for the future scenarios show high intermodel and interregion variability (Figure S2) and relatively lower ensemble member agreement (Figure S4) as compared to TASMAX. In CAN and MIR, EA and IND display increases in the frequency of light precipitation ($1-2\,mm\,day^{-1}$), whereas the other three models show a reduction, which is consistent with previous studies (e.g., Kitoh et al., 2013; Seneviratne et al., 2012). Only AUS (Figures S2k–S2o) shows a consistent reduction in the frequency of light precipitation across models. The future projections of light rainfall frequency is likely to change for Plus-2.0 and Plus-1.5 scenarios compared to All-Hist, but is about as likely to change as not for the additional 0.5°C warming (Figure S4). As the mean annual precipitation in AUS decreases in Plus-1.5 (Figure 4g), this indicates an increase in the frequency of dry days, which has been shown in other climate simulations (Reisinger et al., 2014). Over EA (Figures S2a–S2e) and IND (Figures S2f–S2j), Plus-1.5 and Plus-2.0 almost uniformly project an increase in the frequency of heavy precipitation ($>16\,mm\,day^{-1}$) compared to All-Hist with high confidence and is likely (Figures S4a–S4e and S4f–S4j), associated with the increase in annual-mean precipitation (Figures 4f–4h). There is low confidence in changes of precipitation extreme over AUS (Figures S4k–S4o) in Plus-2.0 scenario, but there is reduced frequency of heavy precipitation in Plus-1.5 (high confidence, likely) and an increase with the extra 0.5°C warming (high confidence, likely). Thus, it is likely that Plus-2.0 produces more frequent heavy precipitation than in Plus-1.5 (>3%) for all AAMR, which suggests very high confidence in heavy precipitation events becoming more frequent with an additional 0.5°C warming.

To further analyze changes in extreme precipitation, we calculate the 70–100th percentiles of daily precipitation for each region (Figure 9) and corresponding ensemble member agreement with the change in
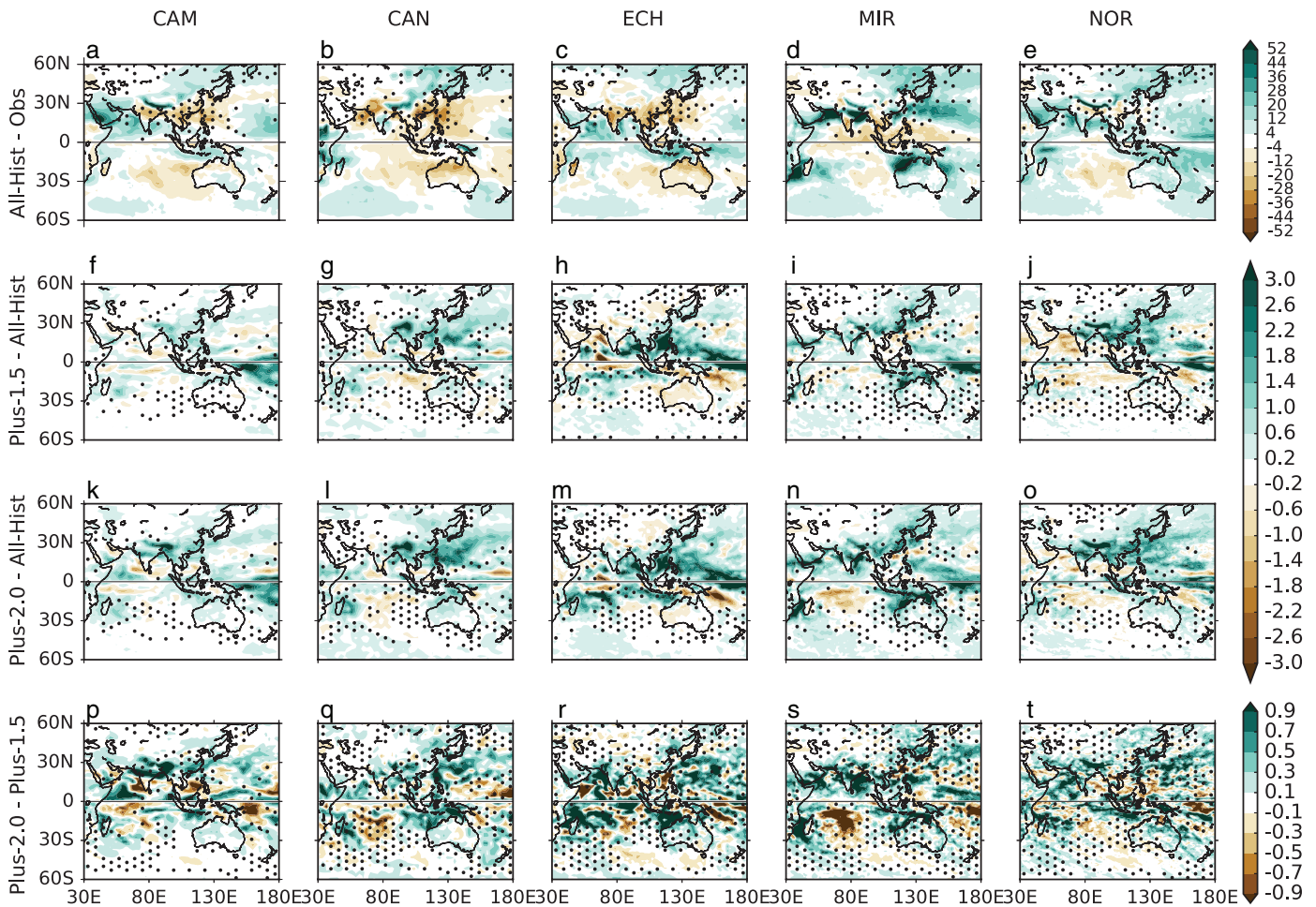
Figure 8. As in Figure 7, but for the change in the 99th percentile of daily precipitation over the monsoon season (mm day⁻¹), with NH showing changes in JJA and SH showing changes in DJF. Note that this introduces a break in the data at the equator, where the season changes. Observations in (a–e) are GPCP.

ensemble mean for 90–100th percentiles (Figure S5). ECH simulates lower values relative to other models for all percentiles, with values less than 70 mm day⁻¹ in all scenarios (Figures 9c, 9h, and 9m) and also shows lower likelihood in the sign of change (Figures S5c, S5h, and S5m). There is high confidence in the increase of extreme precipitation intensities (>90th percentile) in Plus-1.5 and Plus-2.0 over the AAMR; these increases are virtually certain over EA (Figures S5a–S5e) and likely over IND (Figures S5f–S5j) and AUS (Figures S5k–S5o). Precipitation intensity increases sharply beyond the 80th percentile for EA and IND in all models except ECH. In AUS, precipitation intensities beyond the 95th percentile only show increases in the future scenarios, with CAN and ECH projecting increases only beyond the 99th percentile. The intensity of most extreme (>99.99th percentile) precipitation increases by at least 5% with an additional 0.5°C of warming in Plus-2.0 compared to Plus-1.5, which is likely and with high confidence over EA and IND, and is likely but with only medium confidence over AUS. Increases of extreme precipitation are associated with warming over the source regions for monsoon precipitation (Figures 1p–1t) as shown by Turner and Slingo (2009).

Persistent daily extremes often cause more severe impacts (e.g., floods, heatwaves) than shorter-lived events. To estimate persistence, we calculate a "persistence ratio" for daily TASMAX and PR (Figure 10). For TASMAX, this is defined as the fraction of all events above the 90th percentile of All-Hist that have length ≥6 days. For PR, we use a threshold of the 95th percentile of All-Hist and a length of ≥5 days. Persistence ratios are computed for each experiment. Changes between All-Hist versus Plus-1.5 and Plus-2.0 are shown as ratios (change ratio), such that change ratio > 1 indicate persistence increases in a future scenario. We
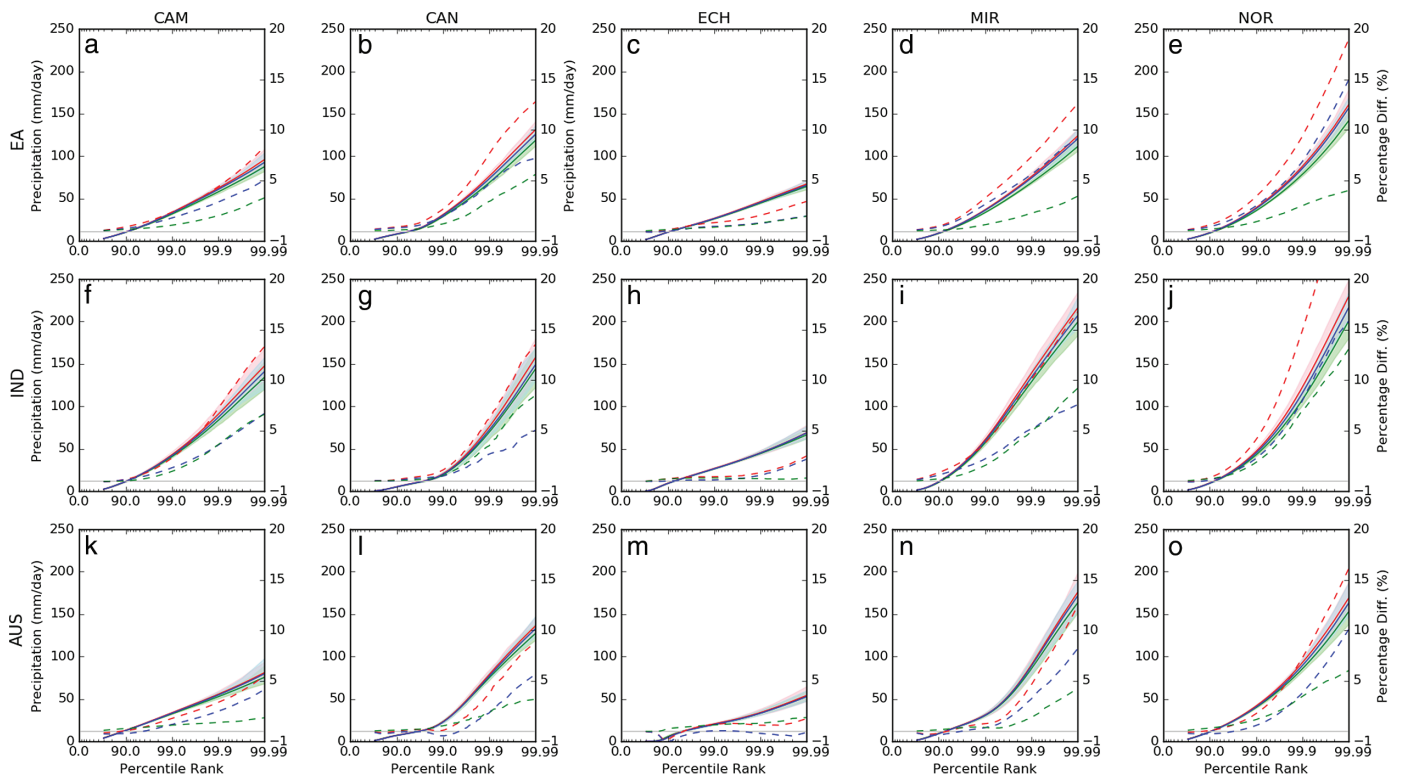
Figure 9. Solid lines show percentiles of daily precipitation (left-hand vertical axis; mm day^{-1}), showing only 70–100th percentiles, for the ensemble means of All-Hist (green), Plus-1.5 (blue) and Plus-2.0 (red) with their respective ensemble ranges shown as transparent envelopes in the same colors. Dashed lines show differences between percentiles (right-hand vertical axis; mm day^{-1}) for Plus-1.5 minus All-Hist (blue), Plus-2.0 minus All-Hist (red) and Plus-2.0 minus Plus-1.5 (green). The horizontal axis is on an inverse logarithmic scale.

also calculate the ensemble member agreement for the change ratio for different scenarios (Figure S6) to understand the likelihood of future change.

For all three scenarios, the TASMAX persistence ratio for EA and IND is higher than for AUS, which suggests more frequent heatwaves in those regions (Figures 10a–10e). Plus-1.5 and Plus-2.0 scenarios experience more frequent persistent events, with particularly large increases in Plus-2.0. EA, IND1, and AUS show increases in TASMAX persistence (≈30%) which has very high confidence and is virtually certain for Plus-2.0 and very likely for Plus-1.5 (Figures S6a–S6e). This increase in persistence combined with the increase in the extreme temperature intensity of these regions (Figure 7) would indicate more frequent heat waves that are also more intense, which can have severe implications for ecology, human health and agriculture (e.g., Alexander & Arblaster, 2009; Burke & Stott, 2017; Im et al., 2017). The difference in projections show an increase of ≈10% in the TASMAX persistence for Plus-2.0 versus Plus-1.5 for EA, AUS (very high confidence, virtually certain) and IND1 (high confidence, likely).

IND has frequent persistent heavy rain events during the summer monsoon in All-Hist (Figures 10f–10j and S6f–S6j), as previously reported (e.g., Turner & Annamalai, 2012). Future scenarios show a very small increase in persistent precipitation events over IND and IND2, but a ≈10% increase over IND1 projected with medium confidence which is likely; there is only a small further increase (≈3%) between Plus-2.0 and Plus-1.5 (medium confidence, likely). AUS shows only small changes in the persistence of heavy precipitation events in the future scenarios, with high intermodel variability and low confidence in projections. EA1 and EA2 display the largest increases in heavy precipitation persistence (high confidence, likely), with a ≈50% increase in Plus-1.5 and a ≈100% increase in Plus-2.0 (in all models except ECH). Combined with the projected increase in heavy precipitation intensity and frequency (Figures 8 and S2), the amplification of flood risk over EA has high confidence and over IND2 has medium confidence.
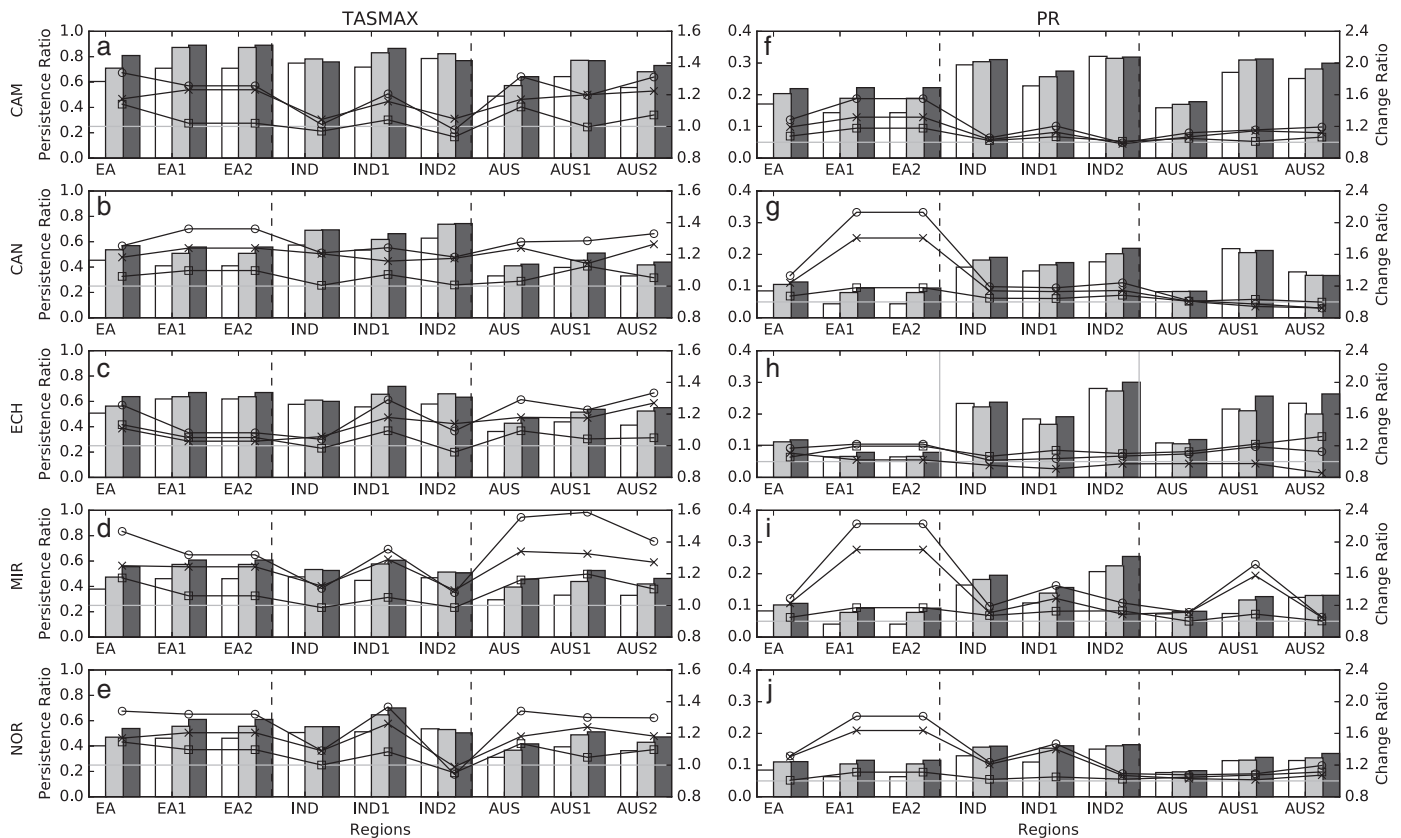
Figure 10. The persistence ratio for All-Hist (white bars), Plus-1.5 (light gray bars) and Plus-2.0 (dark gray bars) corresponding to the left side axis, for variable daily TASMAX in left column and daily precipitation (PR) in the right column for all regions (EA, IND, AUS) and subregions (EA1, EA2, IND1, IND2, AUS1, AUS2). Different models are shown in (a,f) CAM4-2degrree, (b,g) CAN, (c,h) ECH, (d,i) MIR and (e,j) NorESM. The change ratio is the ratio of the persistence ratio between Plus-2.0 and All-Hist (line with circles), Plus-1.5 and All-Hist (line with crosses) and Plus-2.0 and Plus-1.5 (line with squares) corresponding to the right side axis. Please refer to the text for details of the persistence ratio.

There are variations in the change ratios when adjusting the thresholds (continuous number of days of extreme event persistence) for calculating persistence in both TASMAX and PR. When the thresholds are increased, the intensity of the change ratios increases for both TASMAX and PR, and vice versa. Despite this sensitivity, the variations in the change ratios are proportional to the variations in the thresholds for persistence. This suggests altering the thresholds would not change the conclusions of our study, which suggests that, EA, IND1, and AUS (AUS1 and AUS2) show increases in TASMAX persistent events with all thresholds, and EA1, EA2, and IND1 show an increase in PR persisting events with all thresholds.

Forcing mechanisms associated with changes in extreme precipitation differ from those mechanisms associated with the changes in mean precipitation (e.g., Sillmann et al., 2017), with extreme intensity more dependent on the global-mean temperature change (e.g., Pendergrass et al., 2015). Regional extreme precipitation changes are also influenced by temperature changes over the moisture source regions (Turner & Slingo, 2009). To illustrate this change, we calculate PT as in Figure 6, but for the change in the 99th percentile of daily precipitation, PT99 (Figure 11). The change in the extreme precipitation in Plus-1.5 and Plus-2.0, relative to All-Hist, shows a near-linear scaling with global-mean temperatures, globally and for the AAMR. Extreme precipitation intensity is constrained globally by moisture availability (Allen & Ingram, 2002), which increases with the mean global temperature (Allan & Soden, 2008; Held & Soden, 2006). In the tropics, although the response to global warming may lead to weakening circulation (Vecchi et al., 2006), the amplification of extreme precipitation due to enhanced moisture availability in warmer worlds leads to a more linear scaling of extreme precipitation with temperature change than for mean precipitation (Allan & Soden, 2008; Emori & Brown, 2005).
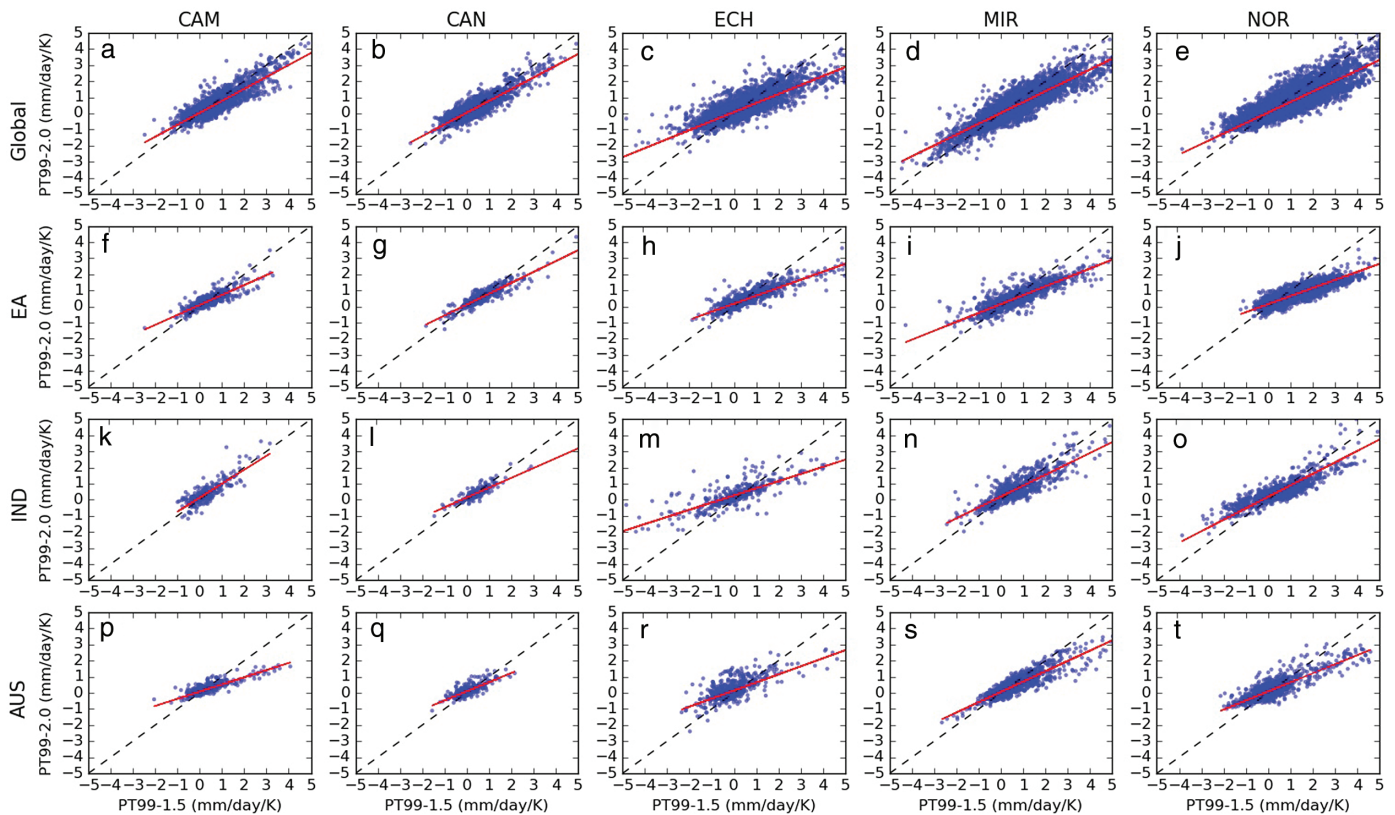
Figure 11. As in Figure 6 for the changes in the 99th percentile of daily precipitation, PT99 ($\Delta p99$/; mm day^{-1} K^{-1}), computed at each grid-point.

4. Conclusions

This study evaluates the effects of 1.5°C and 2.0°C global-mean warming, relative to preindustrial, against a present-day scenario (2006–2015) on mean and extremes over the AAMR, using large ensembles of simulations with five atmospheric general circulation model simulations from the HAPPI project (Table 1). The HAPPI simulations differ from previous analysis of 1.5°C and 2.0°C thresholds in simulations from the CMIP5 because the HAPPI simulations use constant forcing, and thus a constant global-mean temperature. Large ensembles of simulations allow a more robust quantification of the effects of small temperature increases—such as the 0.5°C warming considered here—on regional climate, as well as extremes. The results must be interpreted with a degree of caution, however, due to the limited number of models (five) with substantial biases in their representations of the present-day scenario, which makes it difficult to separate model biases from projected changes.

We summarize our findings for the AAMR in Table 2, including conclusions about the effects of warming (both at 2.0°C and 1.5°C) and the specific effects of an additional 0.5°C warming. We separate the AAMR into three regions, East Asia (EA), India (IND), and Australia (AUS), following Section 2.1 (see Figure 1f). Our conclusions illustrate the some of the key uncertainties in the projected changes, as well as regions and variables for which there is considerable agreement among models. Many of the projections from the HAPPI models support the general consensus of the scientific community regarding changes associated with the warming in the tropics (IPCC, 2014c).

For an additional warming of 0.5°C, there is high confidence and virtual certainty of the projected increase of mean surface temperature ($\approx$0.8°C), as well as high confidence in the increase of intensity (>0.7°C), frequency ($\approx$20%) and persistence ($\approx$10% in EA, IND1, and AUS) of daily extreme temperatures over the AAMR in Plus-2.0 compared to Plus-1.5, which is likely to occur. Restricting warming to 1.5°C would reduce the risk associated with heat stress related impacts, including human heath and spread of infectious diseases (Patz et al., 2005), crop yields over regions like India (Lobell et al., 2012), stress in urbanized environments

Table 2.

Summary of the Key Changes for (left) the Future Warmer Scenarios (Plus-1.5 and Plus-2.0 experiments) and Present-day Conditions (All-Hist experiment); and (right) an Additional 0.5°C Warming (Plus-2.0 Compared to Plus-1.5)

	Future scenarios versus All-Hist	+2.0°C versus +1.5°C
	Mean climate	
TAS	• Significant warming over AAMR in the future scenarios (very high confidence, virtually certain) • Greater warming over the land than the surrounding oceans, with EA warming the most • NH warms more than SH	• Significant warming over AAMR in Plus-2.0 (very high confidence, virtually certain) • Greater warming (≈0.8°C) over the AAMR land than the surrounding oceans • Greater warming (>1.0°C) over higher altitudes (Tibetan Plateau, Himalayas, Western Australia)
PR	• Monsoon precipitation increases considerably over EA (high confidence and likely) and IND (medium confidence, likely) • Annual precipitation increases in EA and IND (high confidence, very likely), but reduces in AUS in Plus-1.5 (high confidence, likely)	• Parts of EA, IND and AUS show coherent increases in monsoon precipitation (high confidence, likely) • Annual precipitation increases in EA and IND (very high confidence, likely). For AUS increases are as likely as decreases
	Daily extremes	
TASMAX	• Intensity of extreme temperature increases significantly over AAMR (very high confidence) • Increased frequency of TASMAX above 300 K (high confidence, likely) and reduced frequency of TASMAX below 300 K (high confidence, as likely as not) • More frequent persistent heat extremes for EA, IND1 and AUS by ≈30% in Plus-2.0 (very high confidence and virtually certain)	• Intensity increases significantly over AAMR (very high confidence), especially over Tibetan Plateau and Gobi Desert • Frequency increases by at least 20% (high confidence, likely) • Persisting extremes become more frequent (≈10%) for all AAMR except IND2 (high confidence, likely)
PR	• Intensity increases significantly for EA, IND (high confidence) and AUS (medium confidence) • Frequency of heavy precipitation reduces for AUS with Plus-1.5 (high confidence, likely); and increases over EA and IND in both Plus-2.0 and Plus-1.5 (very high confidence, likely) • Frequency of persistent extremes increases over EA1, EA2, IND1 (high confidence, likely)	• Intensity of monsoon extremes increases significantly over EA1 and IND1 (high confidence) and the rest of the AAMR (medium confidence) • Increase in the frequency of the extreme precipitation is higher in Plus-2.0 by at least 3% (high confidence, likely) • Frequency of persistent extremes increases over EA1 and EA2 (≈50%, high confidence, likely), and IND1 (≈3%, medium confidence, likely).

Note. Regions referenced in the table are the Asian-Australian Monsoon Region (AAMR) as well as East Asia (EA), India (IND), and Australia (AUS), shown in Figure 1f, as well as the Northern Hemisphere (NH) and Southern Hemisphere (SH).

over expanding cities in developing countries (McCarthy et al., 2010) and loss of ecological niches like coral reefs over Australia (King et al., 2017; Schleussner et al., 2015). Further impact-specific modeling is needed to quantify changes in risk between 1.5°C and 2.0°C.

For EA and IND, our analysis shows that an additional 0.5° warming also increases mean monsoon precipitation. Extreme precipitation frequency over the AAMR (>3%) and persistence over the subregions of EA1, EA2 (≈50%), and IND1 (≈3%) show a likely increase in a 2.0°C warmer world compared to 1.5°C, which will enhance the heavy flood risks in these densely populated regions (Hirabayashi et al., 2013; Milly et al., 2002). These enhanced climatic stresses associated with the additional half a degree of warming will have greater impacts over the vulnerable regions of EA and IND due to their high population density. However,

the effects of 0.5°C warming on precipitation over AUS are much less certain, as are the overall effects of warming, with uncertainty in the sign of the change among models and even among ensemble members of the same model.

This study evaluates the HAPPI experiments for climate projections of 2.0°C versus 1.5°C warmer world over the AAMR. The results highlight the benefit of limiting the global temperature change to 1.5°C over the preindustrial levels, with the severity of impacts increasing with an extra half degree of warming, particularly for temperature and precipitation extremes. Similar analysis over other regions and the estimation of costs associated with the impacts of the additional half a degree of warming will be important for climate policy decisions.

References

Adler, R. F., Huffman, G. J., Chang, A., Ferraro, R., Xie, P.-P., Janowiak, J., et al. (2003). The version-2 global precipitation climatology project (GPCP) monthly precipitation analysis (1979–present). *Journal of Hydrometeorology*, 4(6), 1147–1167. https://doi.org/10.1175/1525-7541(2003)004<1147:TVGPCP>2.0.CO;2

Alexander, L. V., & Arblaster, J. M. (2009). Assessing trends in observed and modelled climate extremes over australia in relation to future projections. *International Journal of Climatology*, 29(3), 417–435. https://doi.org/10.1002/joc.1730

Allan, R. P., & Soden, B. J. (2008). Atmospheric warming and the amplification of precipitation extremes. *Science*, 321(5895), 1481–1484. https://doi.org/10.1126/science.1160787

Allen, M. R., & Ingram, W. J. (2002). Constraints on future changes in climate and the hydrologic cycle. *Nature*, 419(6903), 224–232. https://doi.org/10.1038/nature01092

Bentsen, M., Bethke, I., Debernard, J., Iversen, T., Kirkevåg, A., Seland, Ø., et al. (2013). The norwegian earth system model, NorESM1-M. Part 1: Description and basic evaluation of the physical climate. *Geoscientific Model Development*, 6(3), 687–720. https://doi.org/10.5194/gmd-6-687-2013

Brown, J. R., Moise, A. F., & Colman, R. A. (2017). Projected increases in daily to decadal variability of Asian-Australian monsoon rainfall. *Geophysical Research Letters*, 44(11), 5683–5690. https://doi.org/10.1002/2017GL073217

Burke, C., & Stott, P. (2017). Impact of anthropogenic climate change on the East Asian summer monsoon. *Journal of Climate*, 30(14), 5205–5220. https://doi.org/10.1175/JCLI-D-16-0892.1

Cherchi, A., Alessandri, A., Masina, S., & Navarra, A. (2011). Effects of increased CO_2 levels on monsoons. *Climate Dynamics*, 37(1–2), 83–101. https://doi.org/10.1007/s00382-010-0801-7

Christensen, J. H., Kanikicharla, K. K., Marshall, G., & Turner, J. (2013). Climate phenomena and their relevance for future regional climate change. In *Climate Change 2013: The Physical Science Basis* (pp. 1217–1308). Cambridge, England and New York: Cambridge University Press.

Collins, M., Knutti, R., Arblaster, J., Dufresne, J.-L., Fichefet, T., Friedlingstein, P., et al. (2013). Long term climate change: Projections, commitments and irreversibility. In *Climate Change 2013: The Physical Science Basis* (pp. 1029–1136). Cambridge, England and New York: Cambridge University Press.

Dee, D. P., Uppala, S., Simmons, A., Berrisford, P., Poli, P., Kobayashi, S., et al. (2011). The era-interim reanalysis: Configuration and performance of the data assimilation system. *Quarterly Journal of the Royal Meteorological Society*, 137(656), 553–597. https://doi.org/10.1002/qj.828

Emori, S., & Brown, S. J. (2005). Dynamic and thermodynamic changes in mean and extreme precipitation under changed climate. *Geophysical Research Letters*, 32(17). https://doi.org/10.1029/2005GL023272

Hallegatte, S., Rogelj, J., Allen, M., Clarke, L., Edenhofer, O., Field, C. B., et al. (2016). Mapping the climate change challenge. *Nature Climate Change*, 6(7), 663–668. https://doi.org/10.1038/nclimate3057

He, B., Yang, S., & Li, Z. (2016). Role of atmospheric heating over the South China Sea and western Pacific regions in modulating Asian summer climate under the global warming background. *Climate Dynamics*, 46(9–10), 2897–2908. https://doi.org/10.1007/s00382-015-2739-2

Held, I. M., & Soden, B. J. (2006). Robust responses of the hydrological cycle to global warming. *Journal of Climate*, 19(21), 5686–5699. https://doi.org/10.1175/JCLI3990.1

Hijioka, Y., Lin, E., Pereira, J., Corlett, R., Cui, X., Insarov, G., et al. (2014). Asia. In *Climate Change 2014: Impacts, Adaptation, and Vulnerability. Part B: Regional Aspects* (pp. 1371–1438). Cambridge, England and New York: Cambridge University Press.

Hirabayashi, Y., Mahendran, R., Koirala, S., Konoshima, L., Yamazaki, D., Watanabe, S., et al. (2013). Global flood risk under climate change. *Nature Climate Change*, 3(9), 816–821. https://doi.org/10.1038/nclimate1911

Hsu, P.-C., Li, T., Luo, J.-J., Murakami, H., Kitoh, A., & Zhao, M. (2012). Increase of global monsoon area and precipitation under global warming: A robust signal? *Geophysical Research Letters*, 39(6). https://doi.org/10.1029/2012GL051037

Hsu, P.-C. (2016). Global monsoon in a changing climate. In *The Monsoons and Climate Change* (pp. 7–24). Switzerland: Springer.

Hu, Z.-Z., Latif, M., Roeckner, E., & Bengtsson, L. (2000). Intensified Asian summer monsoon and its variability in a coupled model forced by increasing greenhouse gas concentrations. *Geophysical Research Letters*, 27(17), 2681–2684. https://doi.org/10.1029/2000GL011550

Hulme, M. (2016). 1.5°C and climate research after the Paris agreement. *Nature Climate Change*, 6(3), 222–224. https://doi.org/10.1038/nclimate2939

Hulme, M., Zhao, Z.-C., & Jiang, T. (1994). Recent and future climate change in East Asia. *International Journal of Climatology*, 14(6), 637–658. https://doi.org/10.1002/joc.3370140604

Im, E.-S., Pal, J. S., & Eltahir, E. A. (2017). Deadly heat waves projected in the densely populated agricultural regions of south asia. *Science Advances*, 3(8), e1603322. https://doi.org/10.1126/sciadv.1603322

IPCC. (2014a). *Climate Change 2014: Synthesis Report. Contribution of Working Groups I, II and III to the Fifth Assessment Report of the Intergovernmental Panel on Climate Change*. Geneva, Switzerland: World Meteorological Organization.

IPCC. (2014b). *Climate Change 2013: The Physical Science Basis: Working Group I Contribution to the Fifth Assessment Report of the Intergovernmental Panel on Climate Change*. Geneva, Switzerland: World Meteorological Organization.

IPCC (2014c). Climate change 2014: Impacts, adaptation, and vulnerability. summaries, frequently asked questions, and cross-chapter boxes. In *A Contribution of Working Group II to the Fifth Assessment Report of the Intergovernmental Panel on Climate Change*. Geneva, Switzerland: World Meteorological Organization.

Irving, D. B., Whetton, P., & Moise, A. F. (2012). Climate projections for Australia: A first glance at CMIP5. *Australian Meteorological and Oceanographic Journal*, *62*(4), 211–225.

Iversen, T., Bentsen, M., Bethke, I., Debernard, J., Kirkevåg, A., Seland, Ø., et al. (2013). The Norwegian earth system model, NorESM1-M. Part 2: Climate response and scenario projections. *Geoscientific Model Development*, *6*(2), 389–415. https://doi.org/10.5194/gmd-6-389-2013

James, R., Otto, F., Parker, H., Boyd, E., Cornforth, R., Mitchell, D., & Allen, M. (2014). Characterizing loss and damage from climate change. *Nature Climate Change*, *4*(11), 938–939. https://doi.org/10.1038/nclimate2411

James, R., Washington, R., Schleussner, C.-F., Rogelj, J., & Conway, D. (2017). Characterizing half-a-degree difference: A review of methods for identifying regional climate responses to global warming targets. *Wiley Interdisciplinary Reviews: Climate Change*, *8*(2).

Jourdain, N. C., Gupta, A. S., Taschetto, A. S., Ummenhofer, C. C., Moise, A. F., & Ashok, K. (2013). The Indo-Australian monsoon and its relationship to enso and iod in reanalysis data and the CMIP3/CMIP5 simulations. *Climate Dynamics*, *41*(11–12), 3073–3102. https://doi.org/10.1007/s00382-013-1676-1

King, A., Karoly, D., & Henley, B. (2017). Australian climate extremes at 1.5°C and 2°C of global warming. *Nature Climate Change*, *7*, 412–416. https://doi.org/10.1038/nclimate3296

Kirkevåg, A., Iversen, T., Seland, Ø., Hoose, C., Kristjánsson, J., Struthers, H., et al. (2013). Aerosol-climate interactions in the Norwegian earth system model-NorESM1-M. *Geoscientific Model Development*, *6*(1), 207–244. https://doi.org/10.5194/gmd-6-207-2013

Kitoh, A., Endo, H., Krishna Kumar, K., Cavalcanti, I. F., Goswami, P., & Zhou, T. (2013). Monsoons in a changing world: A regional perspective in a global context. *Journal of Geophysical Research: Atmospheres*, *118*(8), 3053–3065. https://doi.org/10.1002/jgrd.50258

Knutti, R., Rogelj, J., Sedláček, J., & Fischer, E. M. (2016). A scientific critique of the two-degree climate change target. *Nature Geoscience*, *9*(1), 13–18. https://doi.org/10.1038/ngeo2595

Lee, J.-Y., & Wang, B. (2014). Future change of global monsoon in the CMIP5. *Climate Dynamics*, *42*(1–2), 101–119. https://doi.org/10.1007/s00382-012-1564-0

Lewis, S. C., King, A. D., & Mitchell, D. M. (2017). Australia's unprecedented future temperature extremes under Paris limits to warming. *Geophysical Research Letters*, *44*(19), 9947–9956. https://doi.org/10.1002/2017GL074612

Lobell, D. B., Sibley, A., & Ortiz-Monasterio, J. I. (2012). Extreme heat effects on wheat senescence in India. *Nature Climate Change*, *2*(3), 186–189. https://doi.org/10.1038/nclimate1356

May, W. (2011). The sensitivity of the Indian summer monsoon to a global warming of 2°C with respect to pre-industrial times. *Climate Dynamics*, *37*(9), 1843–1868. https://doi.org/10.1007/s00382-010-0942-8

McCarthy, M. P., Best, M. J., & Betts, R. A. (2010). Climate change in cities due to global warming and urban effects. *Geophysical Research Letters*, *37*(9). https://doi.org/10.1029/2010GL042845

Menon, A., Levermann, A., Schewe, J., Lehmann, J., & Frieler, K. (2013). Consistent increase in Indian monsoon rainfall and its variability across CMIP-5 models. *Earth System Dynamics*, *4*, 287–300. https://doi.org/10.5194/esd-4-287-2013

Milly, P. C. D., Wetherald, R. T., Dunne, K., & Delworth, T. L. (2002). Increasing risk of great floods in a changing climate. *Nature*, *415*(6871), 514–517. https://doi.org/10.1038/415514a

Mitchell, D., AchutaRao, K., Allen, M., Bethke, I., Beyerle, U., Ciavarella, A., et al. (2017). Half a degree additional warming, prognosis and projected impacts (HAPPI): Background and experimental design. *Geoscientific Model Development*, *10*(2), 571–583. https://doi.org/10.5194/gmd-10-571-2017

Mitchell, D., James, R., Forster, P. M., Betts, R. A., Shiogama, H., & Allen, M. (2016). Realizing the impacts of a 1.5°C warmer world. *Nature Climate Change*, *6*(8), 735–737. https://doi.org/10.1038/nclimate3055

Morice, C. P., Kennedy, J. J., Rayner, N. A., & Jones, P. D. (2012). Quantifying uncertainties in global and regional temperature change using an ensemble of observational estimates: The HadCRUT4 data set. *Journal of Geophysical Research: Atmospheres*, *117*(D8). https://doi.org/10.1029/2011JD017187

Neale, R. B., Richter, J., Park, S., Lauritzen, P. H., Vavrus, S. J., Rasch, P. J., & Zhang, M. (2013). The mean climate of the community atmosphere model (cam4) in forced sst and fully coupled experiments. *Journal of Climate*, *26*(14), 5150–5168. https://doi.org/10.1175/JCLI-D-12-00236.1

Patz, J. A., Campbell-Lendrum, D., Holloway, T., & Foley, J. A. (2005). Impact of regional climate change on human health. *Nature*, *438*(7066), 310–317. https://doi.org/10.1038/nature04188

Pendergrass, A. G., Lehner, F., Sanderson, B. M., & Xu, Y. (2015). Does extreme precipitation intensity depend on the emissions scenario? *Geophysical Research Letters*, *42*(20), 8767–8774. https://doi.org/10.1002/2015GL065854

Pepin, N., Bradley, R., Diaz, H., Baraër, M., Caceres, E., Forsythe, N., et al. (2015). Elevation-dependent warming in mountain regions of the world. *Nature Climate Change*, *5*(5), 424–430.

Reichler, T., & Kim, J. (2008). How well do coupled models simulate today's climate? *Bulletin of the American Meteorological Society*, *89*(3), 303–311. https://doi.org/10.1175/BAMS-89-3-303

Reick, C., Raddatz, T., Brovkin, V., & Gayler, V. (2013). Representation of natural and anthropogenic land cover change in mpi-esm. *Journal of Advances in Modeling Earth Systems*, *5*(3), 459–482. https://doi.org/10.1002/jame.20022

Reisinger, A., KRL, Chiew, F., Hughes, L., Newton, P., Schuster, S., et al. (2014). Australasia. In *Climate Change 2014: Impacts, Adaptation, and Vulnerability. Part B. Regional Aspects* (pp. 1371–1438). Cambridge, England and New York: Cambridge University Press.

Rogelj, J., Den Elzen, M., Höhne, N., Fransen, T., Fekete, H., Winkler, H., et al. (2016). Paris agreement climate proposals need a boost to keep warming well below 2°C. *Nature*, *534*(7609), 631–639. https://doi.org/10.1038/nature18307

Rogelj, J., & Knutti, R. (2016). Geosciences after Paris. *Nature Geoscience*, *9*(3), 187–189. https://doi.org/10.1038/ngeo2668

Sandeep, S., & Ajayamohan, R. S. (2015). Poleward shift in Indian summer monsoon low level jetstream under global warming. *Climate Dynamics*, *45*(1), 337–351. https://doi.org/10.1007/s00382-014-2261-y

Schleussner, C., Lissner, T., Fischer, E. M., Wohland, J., Perrette, M., Golly, A., et al. (2015). Differential climate impacts for policy-relevant limits to global warming: The case of 1.5°C and 2°C. *Earth System Dynamics Discussions*, *6*, 2447–2505. https://doi.org/10.5194/esdd-6-2447-2015

Schneider, T., O'Gorman, P. A., & Levine, X. J. (2010). Water vapor and the dynamics of climate changes. *Reviews of Geophysics*, *48*(3). https://doi.org/10.1029/2009RG000302

Seneviratne, S. I., Donat, M. G., Pitman, A. J., Knutti, R., & Wilby, R. L. (2016). Allowable CO2 emissions based on regional and impact-related climate targets. *Nature*, *529*(7587), 477–483. https://doi.org/10.1038/nature16542

Seneviratne, S. I., Nicholls, N., Easterling, D., Goodess, C. M., Kanae, S., Kossin, J., et al. (2012). Changes in climate extremes and their impacts on the natural physical environment. In *A Special Report of Working Groups I and II of the Intergovernmental Panel on Climate Change (IPCC)* (pp. 109–230). Cambridge, England and New York: Cambridge University Press.

Shiogama, H., Watanabe, M., Imada, Y., Mori, M., Kamae, Y., Ishii, M., & Kimoto, M. (2014). Attribution of the June-July 2013 heat wave in the southwestern United States. *Solaiat*, *10*, 122–126. https://doi.org/10.2151/sola.2014-025

Sillmann, J., Stjern, C. W., Myhre, G., & Forster, P. M. (2017). Slow and fast responses of mean and extreme precipitation to different forcing in CMIP5 simulations. *Geophysical Research Letters*, *44*(12), 6383–6390. https://doi.org/10.1002/2017GL073229

Sperber, K., Cusiner, E., Kitoh, A., Mechoso, C., Moise, A., Moufouma-Okia, W., et al. (2017). Modelling monsoons. In *The Global Monsoon System—Research and Forecast. World Scientific Series on Asia-Pacific Weather and Climate* (pp. 79–100). Singapore: World Scientific.

Sperber, K. R., Annamalai, H., Kang, I.-S., Kitoh, A., Moise, A., Turner, A., et al. (2013). The Asian summer monsoon: An intercomparison of CMIP5 vs. CMIP3 simulations of the late 20th century. *Climate Dynamics*, *41*(9–10), 2711–2744. https://doi.org/10.1007/s00382-012-1607-6

Stevens, B., Giorgetta, M., Esch, M., Mauritsen, T., Crueger, T., Rast, S., et al. (2013). Atmospheric component of the mpi-m earth system model: Echam6. *Journal of Advances in Modeling Earth Systems*, *5*(2), 146–172. https://doi.org/10.1002/jame.20015

Tokinaga, H., Xie, S.-P., Deser, C., Kosaka, Y., & Okumura, Y. M. (2012). Slowdown of the walker circulation driven by tropical indo-pacific warming. *Nature*, *491*(7424), 439–443. https://doi.org/10.1038/nature11576

Turner, A. G., & Annamalai, H. (2012). Climate change and the south Asian summer monsoon. *Nature Climate Change*, *2*(8), 587–595. https://doi.org/10.1038/nclimate1495

Turner, A. G., & Slingo, J. M. (2009). Uncertainties in future projections of extreme precipitation in the Indian monsoon region. *Atmospheric Science Letters*, *10*(3), 152–158. https://doi.org/10.1002/asl.223

United Nations Framework Convention of Climate Change (2015). *Paris Agreement*, United Nations. Retrieved from http://unfccc.int/files/essential_background/convention/application/pdf/english_paris_agreement.pdf

Vecchi, G. A., Soden, B. J., Wittenberg, A. T., Held, I. M., Leetmaa, A., & Harrison, M. J. (2006). Weakening of tropical pacific atmospheric circulation due to anthropogenic forcing. *Nature*, *441*(7089), 73–76. https://doi.org/10.1038/nature04744

von Salzen, K., Scinocca, J. F., McFarlane, N. A., Li, J., Cole, J. N., Plummer, D., et al. (2013). The canadian fourth generation atmospheric global climate model (CanAM4). Part I: Representation of physical processes. *Atmosphere-Ocean*, *51*(1), 104–125. https://doi.org/10.1080/07055900.2012.755610

Wang, B., Ding, Q., Fu, X., Kang, I.-S., Jin, K., Shukla, J., & Doblas-Reyes, F. (2005). Fundamental challenge in simulation and prediction of summer monsoon rainfall. *Geophysical Research Letters*, *32*(15). https://doi.org/10.1029/2005GL022734

Wang, B., Kang, I., & Lee, J. (2004). Ensemble simulations of Asian-Australian monsoon variability by 11 agcms. *Journal of Climate*, *17*(4), 803–818. https://doi.org/10.1175/1520-0442(2004)017<0803:ESOAMV>2.0.CO;2

Wang, B., Liu, J., Kim, H.-J., Webster, P. J., & Yim, S.-Y. (2012). Recent change of the global monsoon precipitation (1979–2008). *Climate Dynamics*, *39*(5), 1123–1135. https://doi.org/10.1007/s00382-011-1266-z

Wang, B., Yim, S.-Y., Lee, J.-Y., Liu, J., & Ha, K.-J. (2014). Future change of Asian-Australian monsoon under RCP 4.5 anthropogenic warming scenario. *Climate Dynamics*, *42*(1–2), 83–100. https://doi.org/10.1007/s00382-013-1769-x

Wang, G., Cai, W., Gan, B., Wu, L., Santoso, A., Lin, X., et al. (2017). Continued increase of extreme El Niño frequency long after 1.5°C warming stabilization. *Nature Climate Change*, *7*(8), 568–572. https://doi.org/10.1038/nclimate3351

Watanabe, M., Suzuki, T., O'ishi, R., Komuro, Y., Watanabe, S., Emori, S., et al. (2010). Improved climate simulation by MIROC5: Mean states, variability, and climate sensitivity. *Journal of Climate*, *23*(23), 6312–6335. https://doi.org/10.1175/2010JCLI3679.1

World Climate Research Programme (2017). *The global monsoon systems*. Retrieved from https://www.wcrp-climate.org/schools/2017/WCRP-JNU_2017/Documents/Papers/monsoon_factsheet.pdf

Zhang, H. (2010). Diagnosing Australia-Asian monsoon onset/retreat using large-scale wind and moisture indices. *Climate Dynamics*, *35*(4), 601–618. https://doi.org/10.1007/s00382-009-0620-x

Zhou, T., Wu, B., Scaife, A. A., Brönnimann, S., Cherchi, A., Fereday, D., et al. (2008). The CLIVAR C20C project: Which components of the Asian-Australian monsoon circulation variations are forced and reproducible? *Climate Dynamics*, *33*(7), 1051.